scientific reports

Check for updates

OPEN

Research on the properties of polymer stabilized coal gangue materials in rubber powder slag base

Zhenxia Li[1,2,3,4], Tengteng Guo[1,2,3,4], Chenze Fang[1,2,3,4], Yuanzhao Chen[1,2,3,4]✉ & Jiaxin Nie[1]

In order to solve the problems of high energy consumption in cement production, environmental pollution by coal gangue, shortage of aggregate resources in road engineering, and improvement of shrinkage performance of semi-rigid base materials, the properties of rubber powder slag-based polymer stabilized coal gangue materials were studied. On the basis of raw material tests, the mechanical properties and durability of slag-based geopolymer stabilized materials with different geopolymer content and coal gangue substitution rate were studied. The unconfined compressive strength, indirect tensile strength, compressive rebound modulus, freeze–thaw and dry shrinkage tests of geopolymer stabilized crushed stone/coal gangue (GSS/GSG) mixtures with different rubber powder contents were carried out. The microstructure of geopolymer stabilized coal gangue mixture was analyzed by scanning electron microscopy and energy spectrum analysis. The results show that with the increase of geopolymer content, the compressive strength, indirect tensile strength and frost resistance of GSS continue to increase, but its drying shrinkage performance will be adversely affected. When coal gangue replaces natural gravel, its performance in all aspects has decreased, and the mechanical properties and frost resistance have decreased significantly. The incorporation of rubber powder will slightly reduce the mechanical properties of geopolymer stabilized coal gangue material, but can effectively improve its drying shrinkage performance. The optimum content of rubber powder is 1.2%, and the dry shrinkage coefficient is reduced by 12.1%. The bonding effect of C–S–H generated by slag can promote the formation of N–A–S–H gel from fly ash. The rubber powder can stabilize the pore of the coal gangue material and the energy absorption of the rubber powder by filling the geopolymer, so as to achieve the purpose of stabilizing the shrinkage performance and compressive resilient modulus of the coal gangue material by the geopolymer.

Keywords Pavement materials, Semi-rigid base material, Geopolymer stable coal gangue, Rubber powder, Microscopic mechanism

With the rapid development of China's economy, the scale of infrastructure has always maintained a high growth. By the end of 2023, the total mileage of expressways in Henan Province was 8300 km. It is expected that by the end of 2025, the total mileage of expressways will exceed 10,000 km. Large-scale infrastructure construction requires the support of the cement industry. The mass production and use of cement not only consumes a lot of energy[1], but also produces high carbon emissions. The comprehensive energy consumption per ton of cement production is about 113.5 kgce[2]. Global greenhouse gas emissions from cement production account for about 5–7%. In addition, harmful gases such as SO_2, NO_X and CO are emitted, causing environmental pollution[3,4]. At the same time, with the rapid advancement of industrialization, the production of industrial waste is also increasing. How to make rational use of these industrial wastes is an important task on the road of green

[1]School of Civil Engineering and Transportation, North China University of Water Resources and Electric Power, Zhengzhou 450045, Henan, China. [2]Henan Province Engineering Technology Research Center of Environment Friendly and High-Performance Pavement Materials, Zhengzhou 450045, Henan, China. [3]Technology Innovation Center of Henan Transport Industry of Utilization of Solid Waste Resources in Traffic Engineering, North China University of Water Resources and Electric Power, Zhengzhou 450045, Henan, China. [4]North China University of Water Resources and Electric Power - Henan Provincial Institute of Transportation Planning and Design Co., Ltd. Green, Low Carbon, and High Performance Road Materials Research and Development Center, Zhengzhou 450045, Henan, China. ✉email: cyz740513@ncwu.edu.cn

sustainable development in China. Geopolymer composites made from industrial wastes such as fly ash, slag and other aluminosilicate materials can help reduce carbon emissions by 80%; this makes geopolymers a green alternative to cement[5,6]. Most of the raw materials of geopolymer come from industrial waste, and compared with traditional Portland cement, it has the characteristics of low carbon emission, fast setting and early strength. Therefore, it can be regarded as an environmentally friendly cementitious material that is more in line with the concept of sustainable development, and has dense, high strength, durability and corrosion resistance. For a long time, China's main energy has been dominated by coal[7–9]. According to statistics, China's total coal consumption in 2022 accounted for 50.6% of the world's total. At the same time, China is also the largest coal importer, with imports close to 6 EJ, and its proportion is far more than the world average. A large amount of solid waste mainly composed of coal gangue is produced in the process of coal production[10]. Due to the low utilization rate of coal gangue, a large part of it is accumulated into mountains and occupies a large area of land resources[11]. The non-biodegradable toxic heavy metal elements contained in coal gangue may be transferred to soil and water. In order to solve these problems, many scholars have carried out a lot of experimental research[12–16]. Raw materials for geopolymers come from a wide range of sources, often including granulated blast furnace slag, fly ash, metakaolin, or rice husk ash. Yi et al.[17] studied the effect of different content and particle size of rice husk ash on the solidified soil of rice husk ash-geopolymer. The results showed that the optimum content of rice husk ash was 10%. During the curing process, sodium silicate hydrate and calcium silicate hydrate gel were produced, filling pores and bonding soil particles to form a complete structure. Liu et al.[18] studied the effect of rice husk on the mechanical properties of metakaolin-based geopolymers in different ways, and determined the optimum preparation conditions of rice husk ash. The results showed that the rice husk ash pretreated by hydrochloric acid contained 98.4% amorphous SiO_2, which made the pore structure of the geopolymer more dense and had higher strength. Ding et al.[19] analyzed the effects of the molar ratio of raw material oxides n (CaO + MgO):n(SiO_2 + Al_2O_3), cement-sand ratio, water glass content and NaOH content on the working performance and mechanical properties of slag-fly ash based geopolymer mortar. Liu et al.[20] prepared a ternary geopolymer by changing the mix ratio of mineral powder, fly ash and metakaolin, and using the compound sodium silicate to excite the alkali, tested its mechanical properties, and analyzed the hydration process through microscopic tests. The results show that the ternary geopolymer is a composite cementitious material mainly composed of C–S–H, C–A–S–H, and N–A–S–H gels formed by the raw materials under the action of alkali-activated hydration. The larger the proportion of mineral powder, the shorter the setting time of the geopolymer, the more calcium-based gels in the hydration products, and the higher the strength of the specimen. The base mixture is one of the main ways of coal gangue road engineering application. Domestic and foreign researchers have done a lot of research on the application of coal gangue to road base[21–23]. Di et al.[24] conducted a preliminary study on the engineering properties of coal gangue through compaction test and triaxial strength test. They systematically analyzed the variation patterns of shear strength parameters, maximum dry density and optimum moisture content of coal gangue with the content of coarse material. Wang et al.[25] studied the influence of vibration mixing process on the performance of cement stabilized coal gangue mixture, and put forward the best conditions and methods of vibration mixing process. Li et al.[26] used waste coal gangue instead of natural stone as road base material. Through the physical, mechanical, chemical and activity tests of coal gangue aggregate, the optimum gradation composition of unconfined compressive strength was determined. Through mechanical test and durability test, it is concluded that the mixture with 4% cement content can not only meet the requirements of early strength of 4.16 MPa, but also show a high-efficiency strength growth rate of 36.10%, showing the best mechanical properties. At the same time, its total shrinkage coefficient is 1.12×10^{-2}, and its anti-drying shrinkage performance is the best. Through the microscopic test, it is concluded that the cement hydration product Ca $(OH)_2$ in the cement stabilized coal gangue mixture reacts with the active SiO_2 and Al_2O_3 in the coal gangue to form the glauberite, which is beneficial to the overall strength and bonding quality of the mixture. Guan et al.[27] also aimed at the possible problems of coal gangue as pavement base, prepared coal gangue by separation and crushing process, and optimized its gradation. The compressive strength test, splitting test, freeze–thaw test and dry shrinkage test of cement stabilized coal gangue with different cement content were carried out, and the test results were compared and analyzed. The results show that the optimum cement content of cement stabilized coal gangue is 4%, which can be used for light traffic base and heavy traffic subbase of secondary and lower highways. Zhang and Fang[28] studied the flexural tensile properties of cement stabilized coal gangue subgrade materials with cement content of 4–7%. The results showed that the flexural tensile strength and flexural tensile modulus increased linearly with the increase of cement content. The cement stabilized coal gangue subgrade material has good flexural tensile properties and is suitable for the base of pavement structure. Zhang et al.[29] studied the effect of cement content on the temperature shrinkage coefficient of cement coal slag stabilized coal gangue base material by electrical measurement method, and compared it with cement stabilized crushed stone and cement stabilized crushed stone. The results show that the temperature shrinkage coefficient of cement coal slag stabilized unburned coal gangue is the largest at − 10 to 20 °C, while the temperature shrinkage coefficient of cement coal slag stabilized spontaneous combustion coal gangue is the largest at − 10 to 0 °C, and the temperature shrinkage coefficient is the smallest when the cement dosage is about 5%. The temperature shrinkage coefficient of cement cinder stabilized coal gangue base material is small, which is suitable for pavement base of road in cold area[30]. Focused on the temperature shrinkage performance of lime-fly ash stabilized coal gangue materials, and explored the feasibility of its application to pavement base in cold regions[31,32].

In summary, geopolymers have the advantages of a wide range of raw materials. Researchers at home and abroad have also conducted a lot of research on the preparation methods and conditions of geopolymers prepared from different raw materials, and have achieved certain research results, mainly including the mechanical properties of geopolymers under different preparation conditions. Frost resistance and shrinkage performance in different environments. In view of the application of coal gangue in semi-rigid base, the mechanical and durability properties of coal gangue are studied from the aspects of mixing process, cement

Experimental parameters	Test result		Specification requirement
Fineness (%)	6.6		≤ 10
Initial setting time (min)	166		≥ 45
Final setting time (min)	237		≤ 600
Stability (min)	1.2		≤ 5
Strength of cement mortar (MPa)			
Break off strength	3d	5.1	≥ 4.0
	28d	8.5	≥ 6.5
Compressive strength	3d	27.3	≥ 21.0
	28d	47.3	≥ 42.5

Table 1. The results of cement test performance.

Index	Unit	Test result	Technical requirement
Apparent specific gravity	/	2.673	≧ 2.45
Moisture content	%	0.24	≧ 1.0
Particle size range < 0.6mm	%	100	100
< 0.15mm	%	99.2	90–100
< 0.075mm	%	91.9	75–100
Appearance	–	Hit to the spot	No agglomerates
Hydrophilic coefficient	–	0.63	< 1

Table 2. Slag powder performance test results.

Component	CaO	SiO_2	Al_2O_3	Fe_2O_3	MgO	SO_3	K_2O	Na_2O
Content (%)	2.32	53.04	34.70	2.53	0.86	0.35	1.76	0.475

Table 3. Chemical composition of fly ash.

dosage and substitution amount at home and abroad, and its feasibility is proved. In addition, researchers at home and abroad have done some research on the mechanical properties and durability of inorganic binder stabilized materials mixed with rubber powder, and achieved satisfactory results. However, at present, there are relatively few studies on the stabilization of coal gangue with geopolymer as cementitious material in China, and due to the nature of semi-rigid base itself, the high water absorption and high pressure crushing value of coal gangue and the toughness of geopolymer are poor. Based on the existing research results, how to improve its shrinkage performance and frost resistance under the premise of taking into account the mechanical properties. Therefore, prolonging its service life is an important problem to be solved urgently. Therefore, this paper studies the slag-based polymer stabilized coal gangue material with rubber powder.

Materials and methods

Materials

Cement

In this experiment, P.O 42.5 ordinary Portland cement produced by a cement Co., Ltd.in Henan was used. According to the requirements of ' Highway Engineering Cement and Cement Concrete Test Procedures' (JTG 3420-2020)[33], the setting time, fineness, stability and mortar strength of the selected cement are tested. The test results are shown in Table 1. All the performance indexes of the selected cement meet the requirements of "Technical Rules for Construction of Highway Pavement Base" (JTG/T F20-2015)[34].

Slag powder

The basic performance test of the selected slag powder raw materials is carried out. The results of the slag powder performance test are shown in Table 2. The properties of the selected slag powder meet the requirements of the specification[34].

Fly ash

Fly ash is a kind of volcanic ash material, which has the ability to improve the working performance of the matrix and improve the deformation resistance and crack resistance of the material. This test uses grade II fly ash produced by a company. The chemical constituents are shown in Table 3.

Test parameters	Test results	Specification requirements
Fineness (%)	9.2	≤ 12
Water demand ratio (%)	91	≤ 105
Water content (%)	0.3	≤ 1
Loss on ignition (%)	3.01	≤ 5
Average particle size (μm)	20.05	/

Table 4. Performance test results of fly ash.

Technology index	Test results				Technical requirements	Test methods
	20–26.5 mm	10–20 mm	5–10 mm	0–5 mm		
Crushing value (%)	–	15.9		–	≦26	T0316
Apparent relative density	2.746	2.736	2.722	2.718	≧2.6	T0304
Water absorption(%)	0.56	0.60	0.69	–	≦2.0	T0304
Needle flake content(%)	6.3	7.5	8.1	–	≦22	T0312
< 0.075 mm particle content (%)	0.41	0.60	0.35	12.91	≦2/≦15	T0310

Table 5. gravel raw material quality test results.

Ingredients (%)	NaOH	Na_2CO_3	Cl	SO_4	N	PO_4	SiO_3	Al	K	Fe
Content (%)	98.1	1.5	0.005	0.005	0.001	0.001	0.01	0.002	0.05	0.326

Table 6. Chemical composition of sodium hydroxide.

The basic performance tests such as fineness, ignition loss and water demand ratio of the fly ash were carried out. The results of the fly ash performance test are shown in Table 4. The test results show that the properties of the selected fly ash meet the requirements of the specification[34].

Gravel

The aggregate used in this test is the gravel aggregate used by a stone factory in Zhengzhou City. It is divided into four blocks according to the particle size, which are 1# (19–26.5 mm), 2# (9.5–19 mm), 3# (4.75–9.5 mm) and 4# (0–4.75 mm). According to the requirements of ' Highway Engineering Aggregate Test Procedure ' JTG E42-2005[35], the basic performance of all gravels in the test is tested. Table 5 is the performance test results of the gravel used in the test.

Coal gangue

The coal gangue used in this paper is taken from the abandoned coal gangue hill in Songcun, Xinmi City, Zhengzhou City, Henan Province. The stone is mostly gray or gray black. Because the rock is large and hard, it is crushed by jaw crusher. After screening, the performance test results of coal gangue are shown in Table 6. The mineral composition of coal gangue is analyzed by XRD, and the results are shown in Fig. 1.

According to the standard spectrum of the material and the XRD test results of the coal gangue in Fig. 1, it can be seen that the strong diffraction peak appears at about $2\theta = 27°$, and the weak diffraction peaks appear near 21°, 37° and 39°, 50°, indicating that the coal gangue is dominated by quartz minerals. The main mineral composition of coal gangue includes quartz, kaolinite, calcite, dolomite, etc.

Alkali activator

The sodium hydroxide used in the test is a solid (white small granular) sodium hydroxide provided by a chemical company. The NaOH content is ≥ 98%, and its chemical composition is shown in Table 6.

Water glass, also known as sodium silicate, as shown in Fig. 2, is an inorganic substance, an aqueous solution of sodium silicate, and a mineral binder. Its chemical formula is $Na_2O{\cdot}nSiO_2$, which is a soluble inorganic silicate. The performance test results are as follows: Table 7.

Rubber powder

Rubber powder is made by crushing waste tires. The common production methods include room temperature chemical method, room temperature crushing method, freezing method and so on. The rubber powder used in this experiment is 60 mesh rubber powder produced by Dujiangyan Huayi Rubber Co., Ltd. The main technical indexes of rubber powder are shown in Table 8.

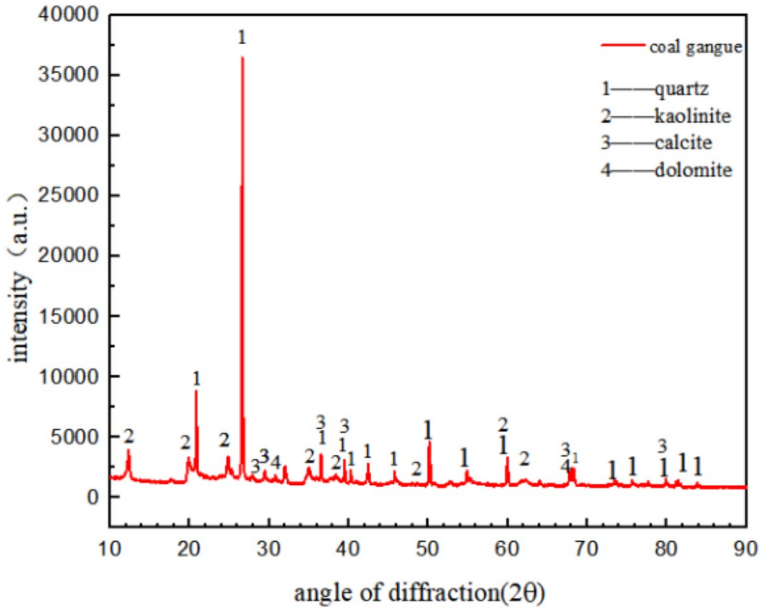

Fig. 1. XRD patterns of coal gangue.

Fig. 2. Appearance of water glass.

Inspection project	Water insoluble (%)	Density (g/cm^3)	SiO_2 (%)	Na_2O (%)	Fe (%)	Modulus
Test results	0.29	1.264	26.2	8.8	0.02	3.07
Technical requirements	≤0.50	1.368–1.394	≥26.0	≥8.2	≤0.05	2.8–3.1

Table 7. Chemical composition of sodium hydroxide.

Mix proportion design

Gradation design

According to the recommended gradation range of C-B-1 used in expressways and first-class highways in Rule[36], the aggregate synthesis gradation of each grade is adjusted according to the screening test results of gravel raw materials. When 1#: 2#: 3#: 4# = 13: 25: 22: 40, it can meet the requirements, and the results are detailed in Fig. 3.

Inspection project	Unit	Detection results	Norm value
60 Mesh screening rate	%	92	≧90
Ash	%	6	≦8
Rubber hydrocarbon content	%	54	≧42
Carbon black content	%	32	≧28
Acetone extract	%	15	≦21
Apparent density	g/cm^3	1.024	/
Natural gum content	%	40.35	/

Table 8. Test results of main technical indexes of rubber powder.

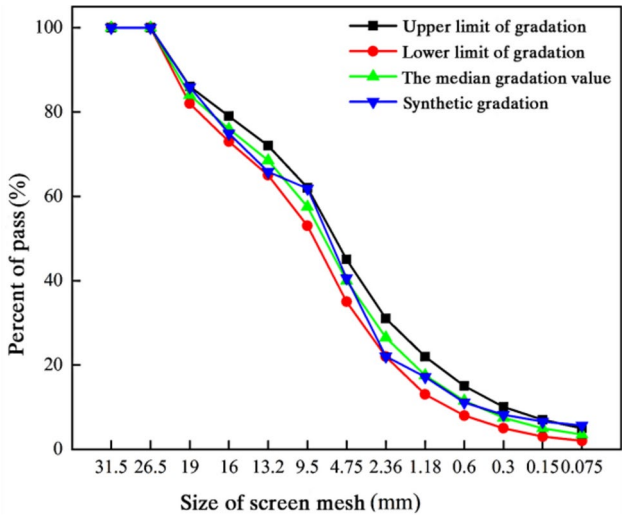

Fig. 3. Synthetic grading curve.

Mix proportion design

The slag powder/fly ash ratio of the slag-based geopolymer prepared in this experiment is 2.5:1, the water glass modulus is 1.2, the alkali activator concentration is 40%, and the water-cement ratio is 0.4. Because the amount of cementitious materials has a great influence on the performance of inorganic binder stabilized materials, the geopolymer content of 3%, 4%, 5%, 6% and 7% was selected, and a set of cement stabilized crushed stone materials with cement content of 5% was set as the control group to study the influence of geopolymer content on the mechanical properties and durability of slag-based GSS. The effects of cement and geopolymer on the properties of inorganic binder stabilized materials were compared and analyzed. Coal gangue with particle size range of 5–10 mm and 10–20 mm was used to replace natural aggregate with 15%, 30% and 45% respectively. Five kinds of geopolymer content were selected to analyze its mechanical properties and durability, and the best replacement amount of coal gangue was obtained. From this, 21 groups of mix ratios are obtained, and the specific mix ratio is shown in Table 9. On the basis of this experimental group, through the unconfined compressive strength test, one of them was selected as the control group, and five groups of rubber powder content (0.3%, 0.6%, 0.9%, 1.2%, 1.5%) from RG-1 to RG-5 were set.

Compaction test

The purpose of compaction test is to determine the maximum dry density of soil and its corresponding optimum water content, which is an indispensable and important test to control the compaction quality of subgrade. According to the test method of 'Test method of inorganic binder stabilized materials for highway engineering' (JTG E51-2009)[36], five kinds of samples with different water contents were prepared, and the compaction test was carried out. The dry density corresponding to the water content was measured by weighing, and the optimum water content at the peak and the corresponding maximum dry density were determined. This experiment adopts C method. Through the heavy compaction test, the maximum dry density and optimal water content of each ratio were obtained. The results are shown in Table 10.

Test method

Analysis of unconfined compressive strength

The specimens were standardly cured for 7, 28 and 60 days. The last day of the curing period was soaked in water, and then the surface water was removed with a dry towel. According to the specification[36], the cement stabilized

Number	Cement (%)	Geopolymer (%)	Natural aggregate (%)	Coal gangue (%)
C-S	5	0	100	0
GSS1	0	3	100	0
GSS2	0	4	100	0
GSS3	0	5	100	0
GSS4	0	6	100	0
GSS5	0	7	100	0
GCG15-1	0	3	85	15
GCG15-2	0	4	85	15
GCG15-3	0	5	85	15
GCG15-4	0	6	85	15
GCG15-5	0	7	85	15
GCG30-1	0	3	70	30
GCG30-2	0	4	70	30
GCG30-3	0	5	70	30
GCG30-4	0	6	70	30
GCG30-5	0	7	70	30
GCG45-1	0	3	55	45
GCG45-2	0	4	55	45
GCG45-3	0	5	55	45
GCG45-4	0	6	55	45
GCG45-5	0	7	55	45

Table 9. Mix proportion design of geopolymer stabilized coal gangue material. CS: Cement stabilized crushed stone; GSS: geopolymer stabilized gravel; GCG: geopolymer stabilized coal gangue.

The amount of cementitious material (%)	3	4	5	6	7
CS					
Maximum dry density (g/cm^3)	–	–	2.291	–	–
Optimum moisture content (%)	–	–	4.4	–	–
GSS					
Maximum dry density (g/cm^3)	2.359	2.388	2.403	2.383	2.374
Optimum moisture content (%)	3.7	3.9	4.0	4.2	4.5
GCG15					
Maximum dry density (g/cm^3)	2.277	2.301	2.352	2.298	2.225
Optimum moisture content (%)	4.1	4.2	4.4	4.5	4.7
GCG30					
Maximum dry density (g/cm^3)	2.143	2.196	2.262	2.324	2.218
Optimum moisture content (%)	4.6	4.7	4.9	5.1	5.2
GCG45					
Maximum dry density (g/cm^3)	2.047	2.113	2.141	2.084	2.033
Optimum moisture content (%)	4.7	4.9	5.0	5.3	5.5

Table 10. Compaction test results.

crushed stone, GSS and geopolymer stabilized coal gangue were subjected to unconfined compressive strength test. During the test, the loading rate was kept at 1 mm/min.

Indirect tensile strength analysis

According to the regulation[36], the indirect tensile strength test of cement stabilized crushed stone, GSS and geopolymer stabilized coal gangue was carried out. During the test, the loading rate of the universal testing machine was controlled at 1 mm/min.

Analysis of compressive resilient modulus

The value of compressive resilience modulus is affected by the type, properties and structure of the material. In this study, the static modulus characteristics of semi-rigid materials are tested by the top surface method in[36]. According to the results of the compressive strength test and the reduction according to the field conditions, the compressive failure load is finally determined to be P. Set the predetermined unit pressure of 0.5P.

Analysis of frost resistance

According to the specification[36], after the specimen is formed, the standard curing is 28 days. On the last day, the specimen is immersed in water, and the water surface does not pass through the top surface of the specimen by 2.5 cm. Then the specimens were taken out, the surface moisture was dried, and the unconfined compressive strength under non-freeze–thaw conditions was tested. The specimen was placed in a low temperature box to ensure that at least 20 mm of voids were left around the specimen to facilitate cold air circulation, and frozen at − 18 °C for 16 h. The time from the completion of the specimen to the temperature drop to − 18 °C should be within (1.5–2.0) h. After one cycle of freezing, weighing, in a 20 °C water tank for 8 h. Then the water on the surface of the sample was dried and weighed again. The above freeze–thaw cycles were repeated until 5 freeze–thaw cycles were completed, and the unconfined compressive strength was measured. After the specimen reaches the specified number of freeze–thaw cycles, the compressive strength (R_{DC}) test after freeze–thaw is carried out.

Dry shrinkage performance analysis

According to the specification[36], the beam was formed by static pressure method, and the sample size was 100 mm × 100 mm × 400 mm. There were 6 samples in each group, of which 3 samples were used to measure the shrinkage deformation, and the other 3 samples were used to measure the drying shrinkage water loss rate. The data were collected by using a dial indicator. The data were recorded once a day for the first 7 days and once every 2 days after 7 days of age. A total of 29 d, 60 d and 90 d data were recorded. And calculate the dry shrinkage strain and dry shrinkage coefficient.

Microscopic test

Using SU8020 HORIBA scanning electron microscope equipped with energy dispersive X-ray spectroscopy (SEM–EDS), the scanning electron microscope test and energy spectrum analysis test were carried out on 7 d and 28 d cement mortar and geopolymer mortar and 7d age GSG30-3 sample. The microstructure of the samples was observed. The samples were subjected to fixed-point analysis, elemental line analysis and elemental surface analysis to determine the surface micro-area composition.

The samples with a particle size of about 10 mm × 10 mm × 5 mm were prepared and dried under vacuum for 24 h. The samples were bonded to the metal table. Before the test, a thin layer of gold was uniformly plated on the surface of the sample. The surface micro-morphology of the sample at four magnifications of 500×, 1000×, 2000× and 5000× was collected by 20 kV acceleration voltage, and the micro-images were output.

Test results and analysis

Unconfined compressive strength

The results of unconfined compressive strength test are shown in Figs. 4, 5, 6, 7 and 8.

Figure 4 shows the compressive strength of different coal gangue substitutions with 5% cementitious material and the development curve of the compressive strength of the cement reference group with the curing age. It can be seen from Fig. 4 that the compressive strength of CS, GSS and GCG increased with the increase of age, and the growth rate slowed down obviously after 28 days, and then the strength increased slowly and tended to be stable. In the early stage of specimen forming, the compressive strength of GSS3 group was much higher than that of CS group, while in the later stage, the compressive strength of GSS3 group was still slightly higher than that of CS group, but the difference was not significant. Specifically, the compressive strength of GSS3 group was 7.76 MPa at 7 d, while that of CS group was 6.69 MPa. At the same amount of cementitious materials, the compressive strength of GSS3 at 7 d, 28 d and 60 d was 16.0%, 5.64% and 2.65% higher than that

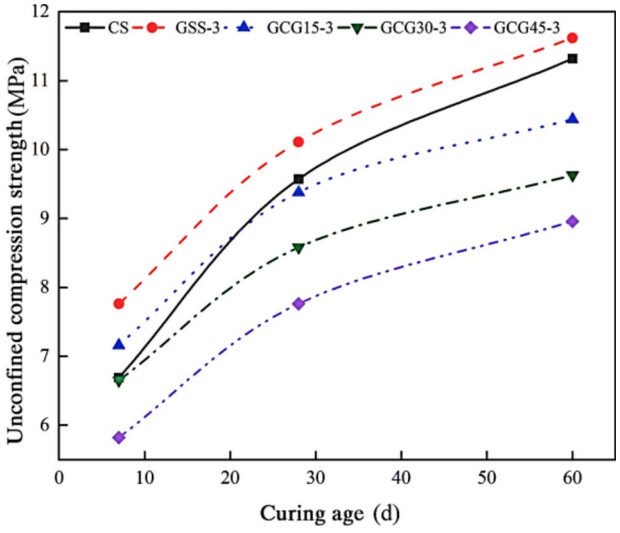

Fig. 4. Unconfined compressive strength of GSS with different mix ratios.

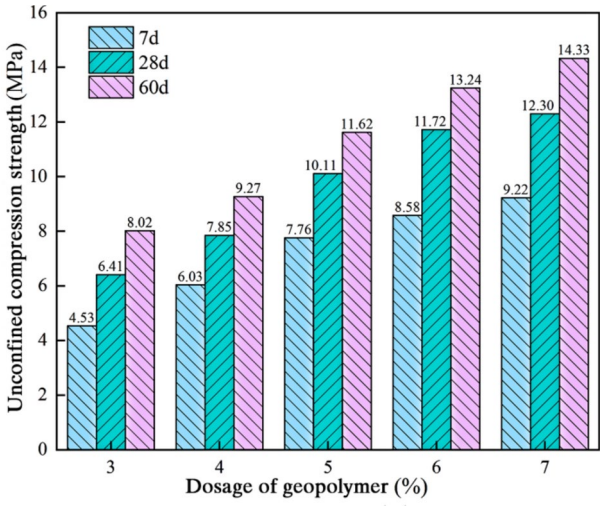

Fig. 5. Unconfined compressive strength of GSS group under different dosage of geopolymer.

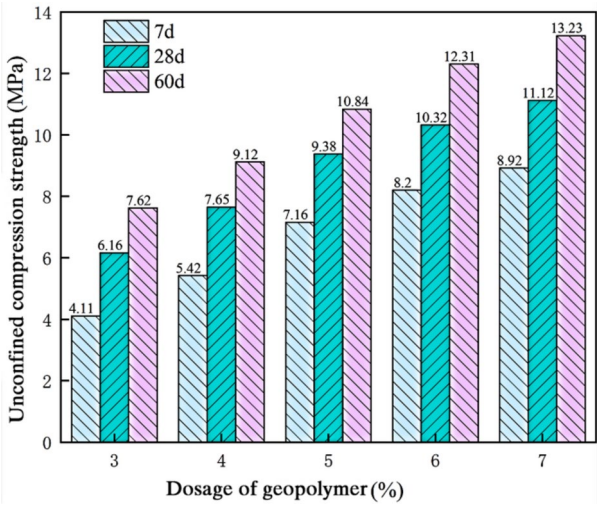

Fig. 6. Unconfined compressive strength of GCG15 group under different dosage of geopolymer.

of CS. The compressive strength of GSS3 group and the turning time of CS group were about 20 days. In the process of strength development, the late strength improvement rate of GSS3 group was lower than that of CS group. This is because the polymerization rate of geopolymer is higher, thus forming more three-dimensional network structure, resulting in the early strength of GSS is higher than that of cement stabilized crushed stone, and the later reaction rate decreases significantly. When the geopolymer is cured at room temperature for 5 h, its compressive strength can reach a high level. If the curing method is more standardized and appropriate, the strength of the geopolymer will further increase with the increase of the age, so it has good early strength characteristics.

Figures 5, 6, 7 and 8 are the compressive strength of geopolymer stabilized coal gangue with different replacement amounts of coal gangue with the change of geopolymer dosage. According to the analysis, with the increase of the amount of geopolymer, the compressive strength of geopolymer stabilized coal gangue with different replacement amounts of coal gangue is continuously improved. The 60 d compressive strength of GSS group, GCG15 group, GCG30 group and GCG45 group is 8.02 MPa, 7.62 MPa, 7.04 MPa and 6.37 MPa respectively when the amount of geopolymer is 3%, and the 60 d compressive strength is 14.33 MPa, 13.23 MPa, 12.19 MPa and 10.76 MPa respectively when the amount of geopolymer is 7%. They increased by 80.9%, 73.6%, 73.1% and 68.9% respectively. This is because as the amount of geopolymer increases, more zeolite precursors (N–A–S–H) and hydrated calcium aluminosilicate gels are formed by the reaction, and more gels exist in the pores between the aggregate surface and the aggregate, so that the cementation strength between the geopolymer and the aggregate is improved, and the integrity is better, so that the strength of the geopolymer stabilized coal gangue is improved.

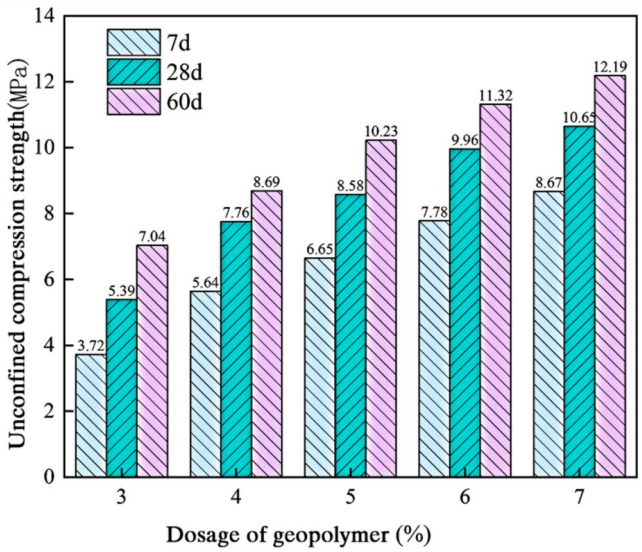

Fig. 7. Unconfined compressive strength of GCG30 group under different dosage of geopolymer.

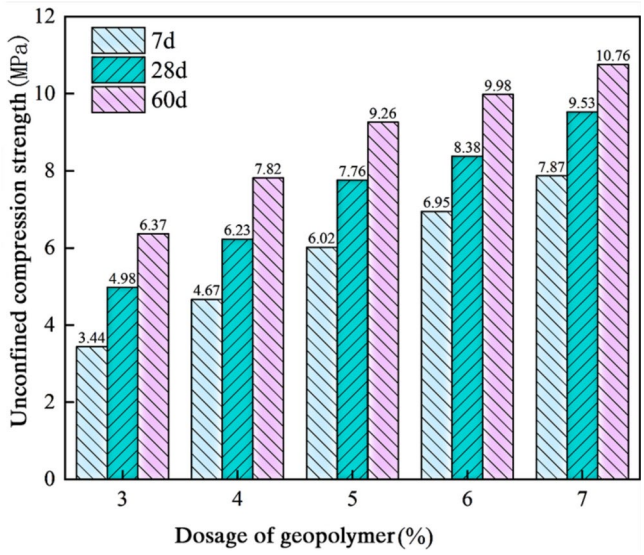

Fig. 8. Unconfined compressive strength of GCG45 group under different dosage of geopolymer.

Further analysis of Figs. 5, 6, 7 and 8 shows that the compressive strength of geopolymer stabilized coal gangue at the same age increases rapidly when the dosage of geopolymer is 3–5%. When the dosage of geopolymer in GSS group, GCG15 group, GCG30 group and GCG45 group increases from 3 to 5%, the compressive strength increases by 44.9%, 42.3%, 45.3% and 45.4% respectively. When the dosage of geopolymer is 6% and 7%, the compressive strength of geopolymer stabilized coal gangue increases by 23.3%, 22.1%, 19.2% and 8.0% respectively compared with that of 5% geopolymer. On the one hand, when the amount of geopolymer is low, the overall alkaline environment in the geopolymer stabilized coal gangue material is weak. In addition, the calcite in natural gravel and coal gangue will dissolve some Si, Ca and Al elements to participate in the geopolymerization reaction, thus further weakening the alkaline environment in the geopolymer stabilized coal gangue material, so that the geopolymerization reaction can generate less gel that can form strength; On the other hand, when the dosage of geopolymer is 3–5%, with the increase of the dosage of geopolymer, the products of geopolymerization reaction increase, so that there are more gel substances between the aggregate surface and the aggregate, and the bonding force between the aggregate and the aggregate increases to form an effective embedded structure, thereby improving the strength of geopolymer stabilized coal gangue materials. However, when the amount of local polymer is too large, it will destroy the interlocking and friction between aggregates to a certain extent. At the same time, it will lead to an increase in the optimal water consumption of geopolymer stabilized coal gangue materials, resulting in a decrease in the degree of compaction, so the strength growth rate slows down.

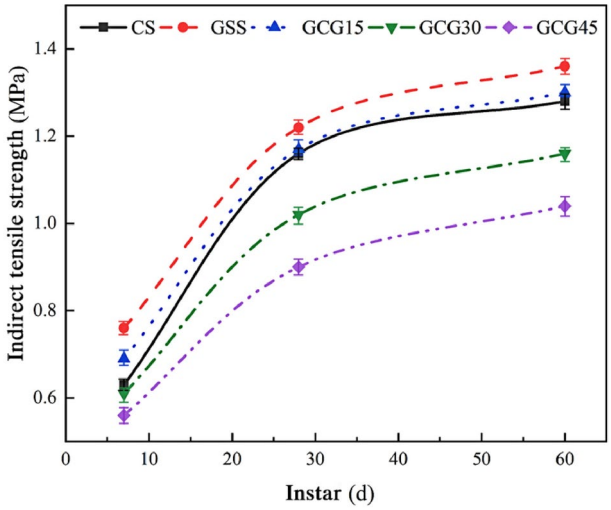

Fig. 9. Indirect tensile strength of GSS with different coal gangue substitution amount.

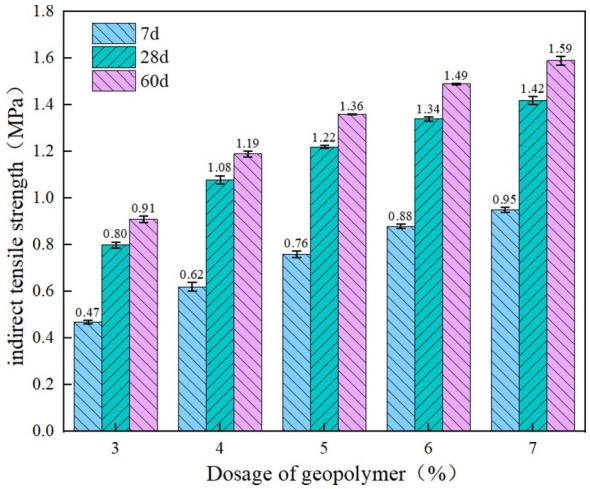

Fig. 10. Indirect tensile strength of GSS group under different dosage of geopolymer.

Through the analysis of the unconfined compressive strength of each group at 7 d, 28 d and 60 d, it is found that the unconfined compressive strength of geopolymer stabilized coal gangue materials with different substitution rates is small when the dosage of geopolymer is 3% and 4%, and the growth rate slows down from 5 to 7%. Therefore, GSG15-3, GSG30-3 and GSG45-3 were selected to explore the influence of different coal gangue substitution rates on the mechanical properties and durability of geopolymer stabilized coal gangue materials. However, the dosage of different geopolymers also affects the mechanical properties and durability of geopolymer stabilized materials. Therefore, GSS1, GSS2, GSS3, GSS4 and GSS5 were selected for subsequent experiments. In addition, GSG30-3 was used as the control group, and five groups of rubber powder content from RG-1 to RG-5 were set (0.3%, 0.6%, 0.9%, 1.2%, 1.5%).

Indirect tensile strength

The results of indirect tensile test for different mix ratios are shown in Figs. 9, 10, 11 and 12.

It can be seen from Fig. 9 that the indirect tensile strength of GSS material is slightly larger than that of cement stabilized crushed stone under the same content of geopolymer instead of cement. When the dosage of geopolymer is 5%, the indirect tensile strength of GSS3 at 7 d age is 0.76 MPa, while that of CS with the same dosage of cementitious material is 0.63 MPa. The former is 20.63% higher than the latter. At the curing age of 28 d and 60 d, the indirect tensile strength of GSS with 5% dosage is 1.22 MPa and 1.36 MPa, respectively, which is 5.23% and 6.25% higher than that of CS, respectively. This is mainly because the strength of geopolymer material is formed faster, and the later strength growth rate is slower than that of cement stabilized crushed stone, which leads to the smaller difference between the later strength of the specimen after geopolymer replacing cement and that of cement stabilized crushed stone. It is still slightly larger than cement stabilized gravel.

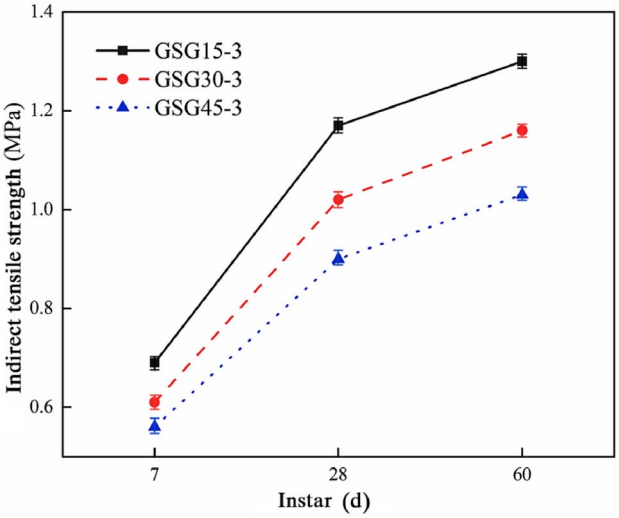

Fig. 11. Indirect tensile strength of GCG45 group under different dosage of geopolymer.

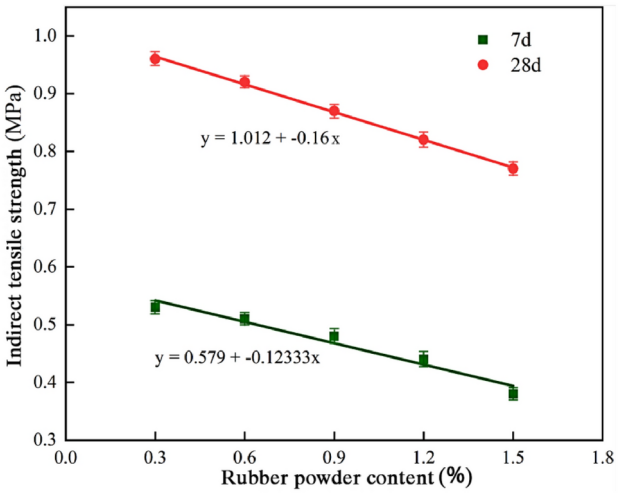

Fig. 12. Indirect tensile strength of mixtures with different rubber powder dosages.

It can be seen from Figs. 10 and 11 that with the increase of coal gangue replacement rate, the change trend of indirect tensile strength and unconfined compressive strength of the specimens is similar, both of which show a downward trend, and the rate of decline gradually increases. The indirect tensile strength of GSS group is the largest under the five kinds of geopolymer dosage, and its strength increases with the increase of geopolymer dosage, which is 0.47 MPa, 0.62 MPa, 0.76 MPa, 0.88 MPa and 0.95 MPa respectively. The indirect tensile strength of GSG45 group was the smallest, and the strength was 0.29 MPa, 0.40 MPa, 0.56 MPa, 0.64 MPa and 0.76 MPa, respectively. Taking 5% geopolymer dosage as an example, the 7 d indirect tensile strength of GCG15, GCG30 and GCG45 groups decreased by 10.14%, 24.59% and 35.71% respectively compared with GSS group with the increase of substitution amount. The indirect tensile strength of 28 d decreased by 4.27%, 19.6% and 35.55% respectively compared with GSS group with the increase of substitution amount. The indirect tensile strength of 60 d decreased by 4.61%, 17.24% and 30.76% respectively compared with GSS group with the increase of substitution amount. The reason for this change trend is similar to that of compressive strength. This is because the internal pores of coal gangue are more and the internal structure is rock bedding, rock joints, coal structure, coal asphalt bedding, which leads to its ability to resist damage when subjected to lateral external force. Relatively low, followed by the fact that the needle-like content of coal gangue is more, the aggregate can not form a better embedded structure, resulting in a decrease in friction and mechanical bite force between the aggregates, which leads to a decrease in the indirect tensile strength of geopolymer-stabilized coal gangue materials. In practical engineering applications, too much coal gangue substitution is more likely to cause cracks in the base. It directly affects the service life of the road.

It can be seen from Fig. 12 that the incorporation of rubber powder has a negative effect on the indirect tensile strength of geopolymer stabilized coal gangue. This is because when the rubber powder is mixed with

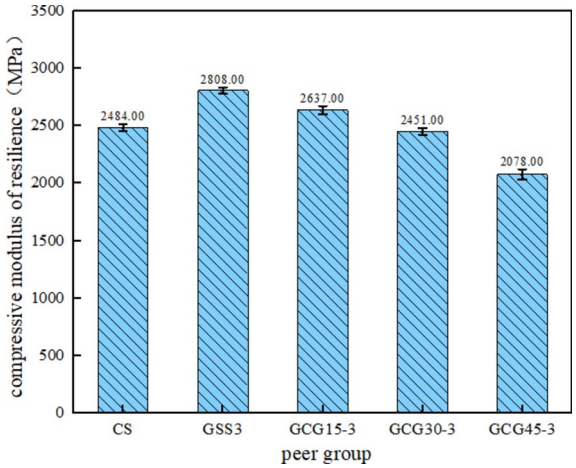

Fig. 13. Test results of compressive resilient modulus with different substitution amounts.

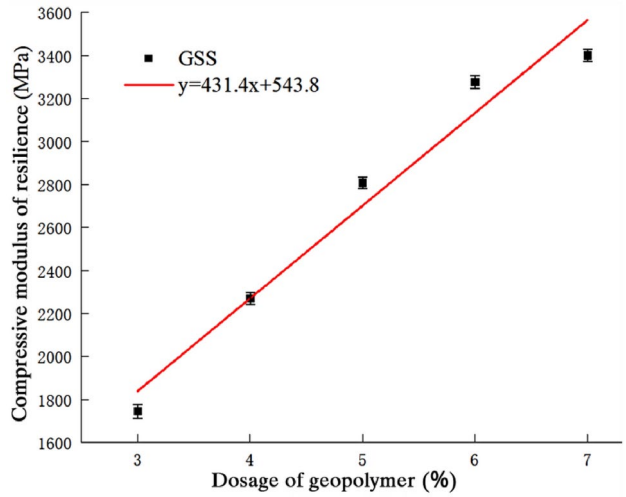

Fig. 14. The variation trend of compressive resilience modulus with different substitution amount of geopolymer content.

the geopolymer stabilized coal gangue, the bonding surface of the mixture will become more complex, resulting in the combination between the rubber powder and the geopolymer and the aggregate is not close enough, and the flexible rubber powder and the rigid aggregate deformation is not coordinated, resulting in a decrease in the overall mechanical properties, which is not conducive to the growth of the splitting strength. When the amount of rubber powder is too large, the rubber powder will also agglomerate, which is easy to crack and damage in the rubber powder aggregation area, resulting in the deformation or damage of geopolymer stabilized coal gangue material under external force or environmental change.

Compressive resilient modulus

The compressive rebound modulus test was carried out for different mix ratios to study the effect of the amount of geopolymer and the amount of coal gangue substitution on the rebound modulus of geopolymer stabilized coal gangue. The test results are shown in Figs. 13 and 14.

According to the analysis of Fig. 13, the compressive resilient modulus of the slag-based polymer stabilized coal gangue material gradually decreases with the increase of the replacement rate of coal gangue. The maximum compressive resilience modulus of the GSS3 group with a substitution amount of 0% is 2808 MPa; the compressive resilient modulus of GCG15-3 group, GCG30-3 group and GCG45-3 group with coal gangue replacement rate of 15%, 30% and 45% and geopolymer dosage of 5% were 2637 MPa, 2451 MPa and 2078 MPa, respectively, which decreased by 6.2%, 12.7% and 26.0% compared with GSS3 group. This is because the elastic modulus of coal gangue is lower than that of natural gravel. Natural gravel usually has good elastic modulus due to its hard stone and stable structure. Due to the inhomogeneity of its composition and structure, the elastic modulus of coal gangue is relatively low, which leads to the weakening of its anti-deformation ability. Secondly, the crushing value of coal gangue is lower than that of natural gravel, and its ability to resist external load is lower. At the

same time, the soft impurity content of the fine soil on the surface of the coal gangue aggregate is large, and the water absorption rate is large, which leads to the increase of the optimal moisture content of the geopolymer stabilized coal gangue material and the decrease of the maximum dry density, which directly affects the degree of compaction and reduces the stiffness of the specimen.

Figure 14 shows the variation of compressive rebound modulus of GSS with the increase of geopolymer content. It can be seen from the diagram that the content of geopolymer has a great influence on the compressive resilient modulus of geopolymer stabilized materials. It can be seen from the fitting that the compressive resilient modulus of slag-based geopolymer stabilized materials increases linearly with the increase of geopolymer content. The content of geopolymer in the GSS group increased from 3 to 7%, and the compressive resilient modulus increased from 1747 to 3401 MPa, an increase of 94.7%. This is due to the increase of the amount of geopolymer, the increase of geopolymerization reaction products, and the formation of more hardened substances. This not only enhances the cohesive force inside the geopolymer stabilized coal gangue material, but also enables the material to better resist deformation when subjected to external forces, and enhances the ability of the material to restore its original state after being subjected to pressure.

The compressive resilient modulus test results of slag-based geopolymer stabilized coal gangue materials with different amounts of rubber powder are shown in Fig. 15.

It can be seen from Fig. 15 that the compressive resilience modulus of geopolymer stabilized coal gangue materials will decrease with the increase of rubber powder content. The compressive resilience modulus of rubber powder content from 0.3 to 1.5% is 2310 MPa, 2194 MPa, 2101 MPa, 2065 MPa, 2011 MPa, respectively, compared with GSG30-3. The modulus decreased by 5.75%, 10.49%, 14.28%, 15.75%, and 17.95%, respectively. It can be seen from the diagram that there is a nonlinear change between 0.3 and 1.5%. This is because the modulus of geopolymer stabilized graded coal gangue mainly depends on the modulus and volume of each component. As a flexible material, the elastic modulus of rubber powder is much smaller than that of geopolymer and aggregate, so that the compressive elastic modulus of geopolymer stabilized coal gangue decreases.

Frost resistance analysis

The results of freeze–thaw test are shown in Fig. 16.

It can be seen from Fig. 16 that the compressive strength loss of the specimens in the GSS3 group was 95.7% after 5 freeze–thaw cycles, and the BDR (The compressive strength loss of the specimen after n freeze–thaw cycles) of the GS group was 95.0%. The GSS3 group was slightly larger than the GS group. This is because the three-dimensional network structure of the geopolymer can effectively resist the erosion of water and ice crystals, reduce the damage of the freeze–thaw cycle to the material structure, and the GSS has higher water stability and durability than cement. Even in the harsh freeze–thaw environment, GSS can maintain good performance stability, and it is not easy to crack and peel off.

With the increase of the amount of geopolymer, the BDR value of geopolymer stabilized macadam increases continuously. The BDR values of GSS1, GSS2, GSS3, GSS4 and GSS5 are 89.4%, 94.3%, 95.7%, 97.0% and 97.4% respectively, and the growth rate decreases gradually. The reason is that the higher amount of geopolymer means that there are more geopolymer pastes in the GSS material to fill the voids between the aggregates, thereby improving the compactness of the GSS material. This helps to reduce the space for water penetration and ice crystal formation, thereby improving the frost resistance of GSS materials to a certain extent.

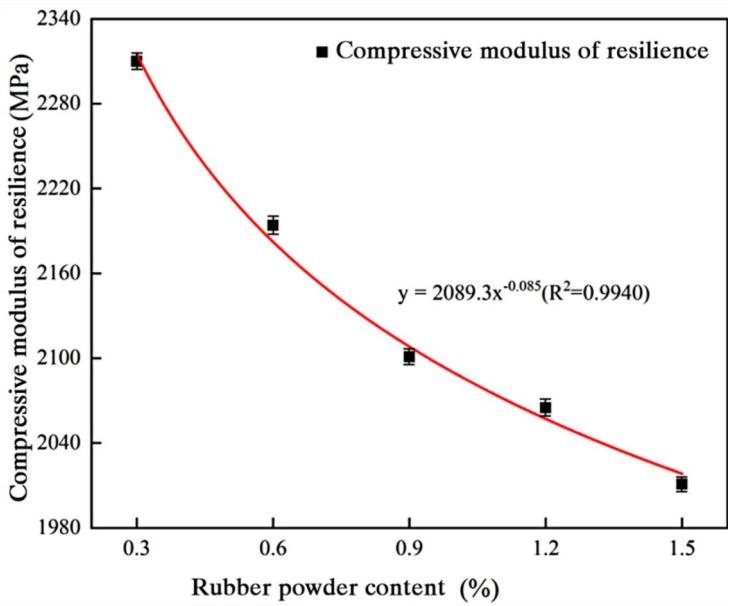

Fig. 15. Compressive rebound modulus of mixtures with different rubber powder dosages.

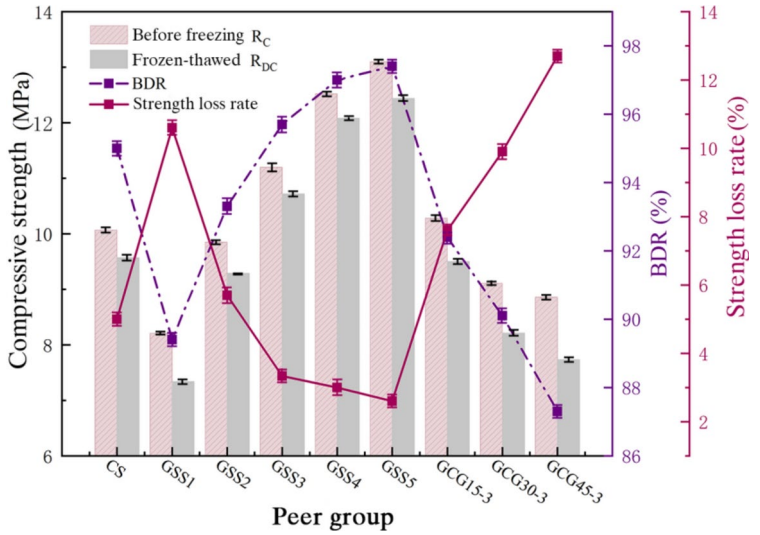

Fig. 16. Freeze–thaw test results of stable materials with different mix ratios.

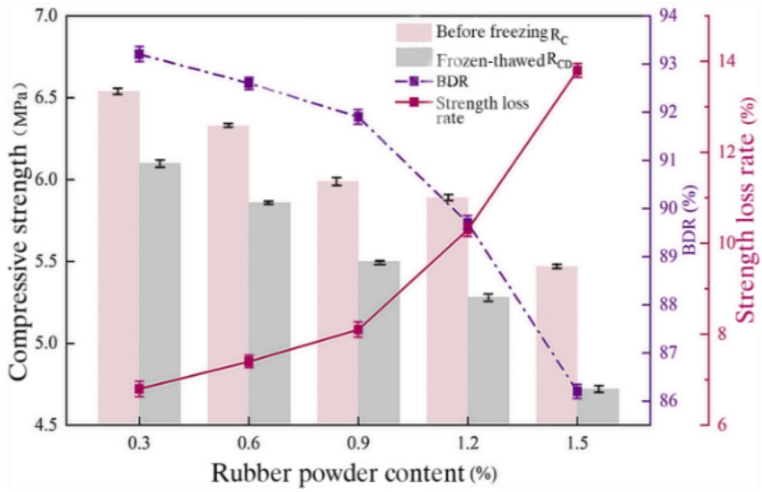

Fig. 17. Freeze–thaw tests on geopolymer stabilized coal gangue materials mixed with rubber powder.

The strength loss rate of geopolymer stabilized coal gangue increased with the increase of coal gangue substitution rate. The BDR values of GCG15-3 group, GCG30-3 group and GCG45-3 group were 92.4%, 90.1% and 87.3%, respectively, which were 3.45%, 5.85% and 8.78% lower than the 95.7% of the reference group. It can be seen that the higher the substitution amount of coal gangue, the faster the BDR value of geopolymer stabilized coal gangue material decreases. This is because the coal gangue itself contains more voids or incompletely burned coal components. With the increase of coal gangue content, the porosity of geopolymer-stabilized coal gangue may increase accordingly, resulting in the formation of weak points or voids inside the geopolymer-stabilized coal gangue material, thereby increasing its permeability and water absorption capacity. During the freeze–thaw cycle, the water in these voids is easy to freeze and expand, and the geopolymer stabilized coal gangue base material cracks.

It can be seen from Fig. 17 that the strength loss rate of geopolymer stabilized coal gangue materials increases with the increase of rubber powder content, and the greater the content of rubber powder, the more obvious the BDR of the mixture decreases. The BDR of RG-1, RG-2, RG-3, RG-4 and RG-5 are 93.2%, 92.6%, 91.9%, 89.7% and 86.2%, respectively. This shows that the incorporation of rubber powder has an adverse effect on the frost resistance of geopolymer stabilized coal gangue materials. Because the bonding between the rubber powder and the geopolymer is not dense, microcracks may occur in the specimen, which further increases the water absorption of the geopolymer stabilized coal gangue material, and finally increases the internal expansion stress, resulting in the loss of strength. Therefore, considering the freeze–thaw cycle durability of geopolymer stabilized coal gangue materials, the rubber powder content should not be too large.

Dry shrinkage age (d)	Dry shrinkage (μm)								
	CS	GSS1	GSS2	GSS3	GSS4	GSS5	GCG15-3	GCG30-3	GCG45-3
1	9	6	7	8	10	12	15	12	12
2	20	14	18	22	24	28	29	25	25
3	32	24	29	37	40	45	41	38	38
4	44	34	39	51	55	63	53	52	52
5	57	45	50	63	69	79	64	66	67
6	70	54	59	75	82	94	75	82	82
7	85	61	68	85	95	107	86	95	99
9	100	67	75	95	107	118	96	107	113
11	113	71	81	104	116	128	105	117	125
13	123	75	88	111	124	136	113	125	135
17	131	82	98	122	136	152	128	140	153
19	138	84	102	127	142	158	134	146	161
21	144	86	106	130	147	163	139	152	168
23	149	88	109	133	152	168	144	157	175
25	154	89	111	135	156	172	147	160	180
27	156	90	113	136	159	176	150	163	185
29	158	91	115	137	162	179	152	165	187
60	160	95	120	142	169	186	157	171	194
90	164	98	122	145	173	190	160	174	197

Table 11. Dry shrinkage of different proportions with age.

Dry shrinkage age (d)	Water loss rate (%)								
	CS	GSS1	GSS2	GSS3	GSS4	GSS5	GCG15-3	GCG30-3	GCG45-3
1	0.82	0.58	0.64	0.70	0.81	0.88	0.75	0.79	0.91
2	1.45	1.04	1.12	1.25	1.45	1.56	1.33	1.39	1.61
3	1.90	1.37	1.48	1.64	1.90	2.04	1.74	1.81	2.10
4	2.22	1.59	1.72	1.91	2.22	2.38	2.03	2.11	2.46
5	2.46	1.77	1.91	2.11	2.47	2.63	2.25	2.34	2.73
6	2.63	1.90	2.06	2.27	2.65	2.83	2.42	2.52	2.92
7	2.74	1.99	2.15	2.37	2.77	2.97	2.54	2.64	3.04
9	2.83	2.06	2.23	2.46	2.87	3.08	2.64	2.74	3.14
11	2.90	2.12	2.30	2.53	2.96	3.17	2.72	2.83	3.23
13	2.97	2.18	2.36	2.59	3.03	3.25	2.79	2.90	3.30
17	3.03	2.23	2.41	2.65	3.09	3.32	2.85	2.97	3.36
19	3.08	2.27	2.45	2.70	3.15	3.38	2.90	3.02	3.42
21	3.12	2.33	2.52	2.78	3.23	3.47	2.98	3.10	3.50
23	3.15	2.36	2.55	2.81	3.26	3.50	3.01	3.14	3.53
25	3.18	2.38	2.57	2.83	3.29	3.53	3.03	3.17	3.56
27	3.21	2.40	2.59	2.86	3.32	3.56	3.05	3.19	3.59
29	3.23	2.42	2.61	2.88	3.34	3.58	3.07	3.22	3.61
60	3.25	2.49	2.68	2.96	3.42	3.67	3.15	3.31	3.69
90	3.33	2.55	2.73	3.01	3.48	3.73	3.22	3.39	3.76

Table 12. The water loss rate of different ratios with age.

Dry shrinkage performance analysis

Tables 11, 12, 13 and 14 are the development of drying shrinkage, water loss rate, drying shrinkage strain and drying shrinkage coefficient of geopolymer stabilized macadam and cement stabilized macadam and geopolymer stabilized coal gangue with age. Figures 18, 19, 20, 21, 22, 23, 24 and 25 show the development of dry shrinkage, water loss rate, dry shrinkage strain and dry shrinkage coefficient of GSS, cement stabilized crushed stone and geopolymer stabilized coal gangue with age.

Dry shrinkage age (d)	Dry shrinkage strain (με)								
	CS	GSS1	GSS2	GSS3	GSS4	GSS5	GCG15-3	GCG30-3	GCG45-3
1	2.26	1.50	1.75	2.00	2.50	3.00	3.75	3.00	3.00
2	5.02	3.51	4.50	5.50	6.01	7.01	7.26	6.26	6.25
3	8.03	6.01	7.26	9.25	10.02	11.26	10.26	9.51	9.50
4	11.04	8.51	9.76	12.76	13.77	15.76	13.26	13.02	13.01
5	17.56	13.52	14.76	18.76	20.53	23.52	18.76	20.53	20.51
6	21.32	15.27	17.02	21.26	23.79	26.77	21.52	23.79	24.76
7	25.09	16.78	18.77	23.76	26.79	29.52	24.02	26.79	28.26
9	28.35	17.78	20.27	26.01	29.04	32.02	26.27	29.29	31.27
11	30.86	18.78	22.02	27.76	31.05	34.03	28.27	31.30	33.77
13	32.87	19.53	23.27	29.26	32.55	36.03	30.27	33.30	36.02
17	34.62	20.53	24.52	30.52	34.05	38.03	32.02	35.05	38.27
19	36.13	21.03	25.53	31.77	35.55	39.53	33.53	36.55	40.27
21	37.38	21.53	26.53	32.52	36.81	40.78	34.78	38.06	42.02
23	38.64	22.03	27.28	33.27	38.06	42.03	36.03	39.31	43.77
25	39.14	22.28	27.78	33.77	39.06	43.03	36.78	40.06	45.02
27	39.64	22.53	28.28	34.02	39.81	44.03	37.53	40.81	46.27
29	40.14	22.78	28.78	34.27	40.56	44.78	38.03	41.31	46.77
60	41.14	23.79	30.03	35.52	42.31	46.53	39.28	42.81	48.52
90	41.65	24.54	30.53	36.27	43.31	47.54	40.03	43.57	49.27

Table 13. Dry shrinkage strain of different proportions changing with age.

Dry shrinkage age (d)	Coefficient of shrinkage (%)								
	CS	GSS1	GSS2	GSS3	GSS4	GSS5	GCG15-3	GCG30-3	GCG45-3
1	2.75	2.59	2.74	2.85	3.08	3.40	5.00	3.81	3.29
2	3.47	3.38	4.01	4.39	4.15	4.49	5.47	4.52	3.89
3	4.23	4.40	4.92	5.64	5.27	5.52	5.90	5.26	4.53
4	4.98	5.34	5.66	6.68	6.19	6.63	6.53	6.17	5.30
5	6.68	7.13	7.18	8.27	7.75	8.31	7.75	8.14	7.03
6	7.79	7.68	7.90	8.95	8.59	9.02	8.48	8.99	8.14
7	8.87	8.14	8.40	9.66	9.34	9.59	9.11	9.76	8.99
9	9.76	8.37	8.80	10.28	9.83	10.10	9.67	10.35	9.68
11	10.39	8.62	9.32	10.71	10.25	10.46	10.14	10.78	10.22
13	10.85	8.77	9.65	11.05	10.52	10.85	10.63	11.22	10.71
17	11.25	9.05	9.99	11.31	10.82	11.26	11.05	11.61	11.20
19	11.58	9.13	10.26	11.59	11.14	11.54	11.40	11.93	11.64
21	11.85	9.22	10.53	11.71	11.39	11.76	11.69	12.26	12.00
23	12.14	9.33	10.71	11.85	11.66	12.01	11.99	12.53	12.39
25	12.20	9.35	10.80	11.91	11.87	12.19	12.13	12.65	12.63
27	12.27	9.38	10.90	11.90	12.01	12.38	12.29	12.78	12.89
29	12.36	9.42	11.02	11.90	12.16	12.51	12.37	12.85	12.96
60	12.36	9.55	11.21	12.02	12.39	12.69	12.45	12.92	13.14
90	12.29	9.64	11.19	12.03	12.45	12.73	12.44	12.84	13.12

Table 14. Dry shrinkage coefficients of different ratios with age.

Different cementitious materials

It can be seen from Fig. 18 that with the increase of dry shrinkage age, the dry shrinkage of GSS GSS3 group and cement stabilized crushed stone CS group increased continuously. The dry shrinkage of cement stabilized macadam increased rapidly in the first 20 days, and the growth rate began to slow down after 20 days. The dry shrinkage of geopolymer stabilized macadam increased rapidly in the first 15 days, and the growth rate began to slow down after 15 days. From the 9th day, the cumulative dry shrinkage of GS group exceeded that of GSS3 group. Table 15 is the fitting equation of dry shrinkage and age. The fitting equation can better reflect the relationship between dry shrinkage and age, and R^2 is greater than 0.99. It can be seen from Fig. 18 that the final water loss rate of GSS3 group with geopolymer as cementitious material is higher than that of CS group

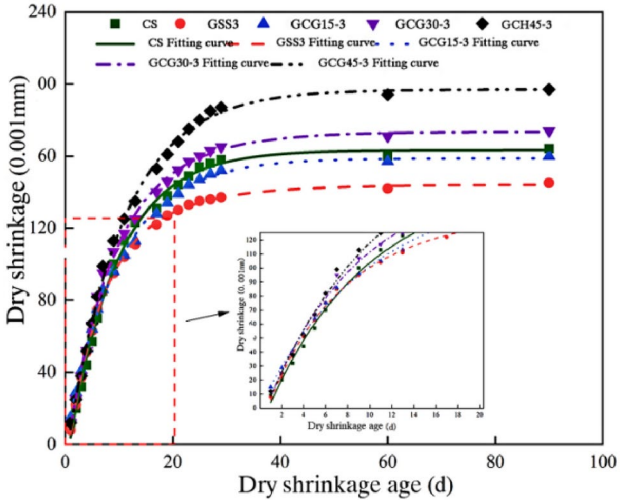

Fig. 18. Curves of dry shrinkage of geopolymer stabilized coal gangue with different substitution amounts with age.

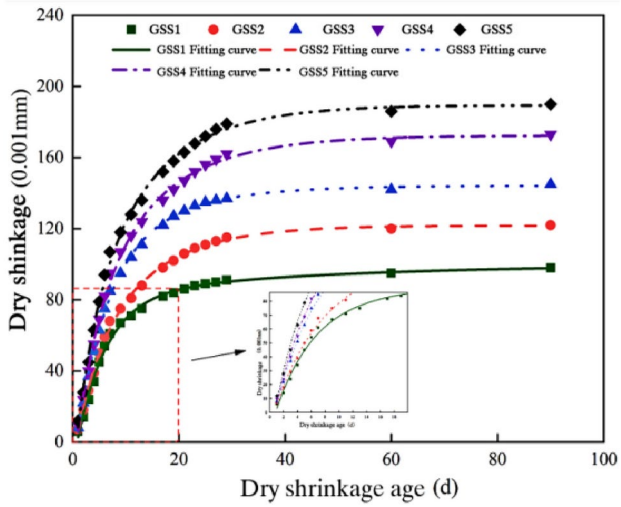

Fig. 19. Curves of dry shrinkage of geopolymer stabilized coal gangue with different dosage of geopolymer with age.

with cement stabilized macadam, and the water loss rate of GSS3 group and CS group increases rapidly in the first 7 days, and the growth rate slows down from 7 to 28 days, and tends to be stable after 28 days. The water loss rate of CS group at 90 days is 3.33% higher than that of GSS group 3.01%. The fitting equation of water loss rate and age in Table 16 can better reflect the relationship between water loss rate and age, and R^2 is greater than 0.99. It can be seen from Fig. 22 that the dry shrinkage strain of GSS is greater than that of cement stabilized crushed stone in the first 6 days. From the 6th day, the dry shrinkage strain of cement stabilized crushed stone exceeds that of GSS. At the age of 90 days, the dry shrinkage strain of CS group is 14.7% higher than that of GSS3 group. The R^2 of the fitting equation shown in Table 17 is greater than 0.98, which can better characterize the development process of dry shrinkage strain with the increase of age. It can be seen from Fig. 24 that the dry shrinkage coefficient of slag-based GSS increases rapidly in the first 19 days, which is higher than that of cement stabilized crushed stone. Then the dry shrinkage coefficient of GSS is overtaken by cement stabilized crushed stone. At the age of 90 days, the total dry shrinkage coefficient of geopolymer stabilized coal gangue is about 4% smaller than that of cement stabilized crushed stone. The R^2 of the fitting equation of dry shrinkage coefficient of inorganic binder stabilized materials with different proportions presented in Table 18 is greater than 0.98, which can better describe the development process of dry shrinkage coefficient with the increase of age.

Comprehensive analysis of the above phenomena, because the early strength of geopolymer develops rapidly, and the geopolymer reaction products form a more stable three-dimensional network structure, which makes the cohesive force between aggregates greater and the integrity better. To a certain extent, it improves the ability to resist shrinkage stress, thereby reducing drying shrinkage; combined with the compaction test results, it can

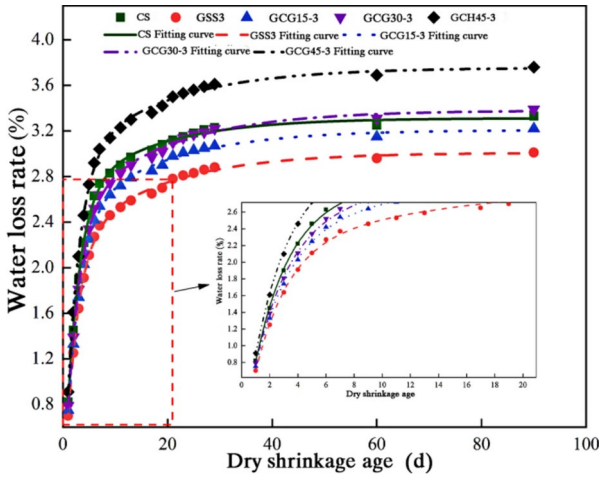

Fig. 20. The curve of water loss rate of rubber powder-geopolymer stabilized coal gangue with age.

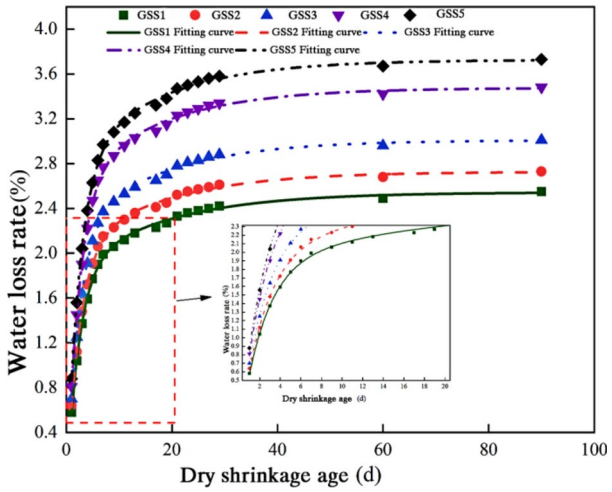

Fig. 21. The curve of water loss rate of geopolymer stabilized coal gangue with different dosage of geopolymer with age.

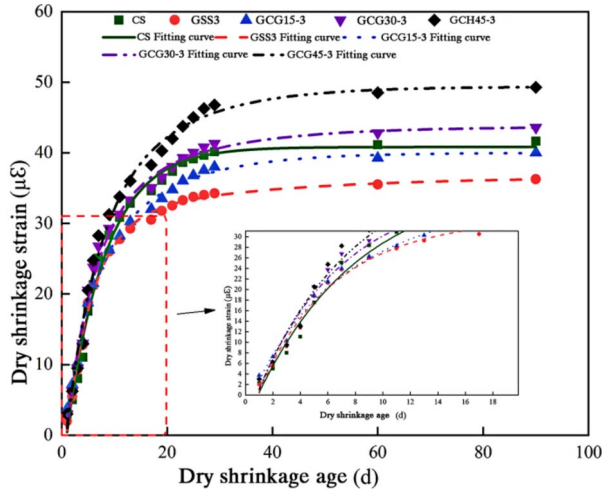

Fig. 22. The curve of dry shrinkage strain with age of different substitution amount.

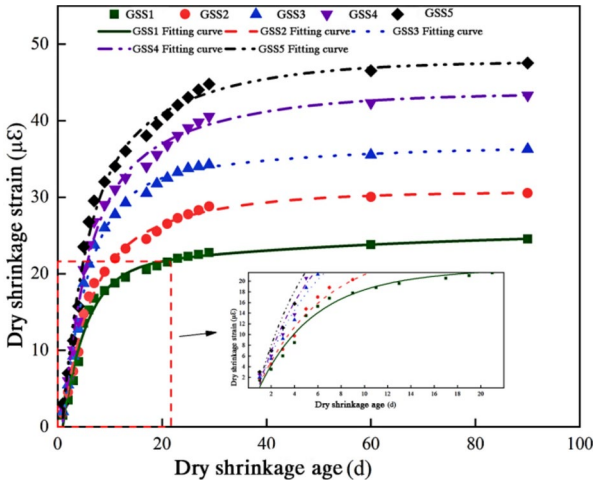

Fig. 23. The curve of dry shrinkage strain with age of different geopolymer dosage.

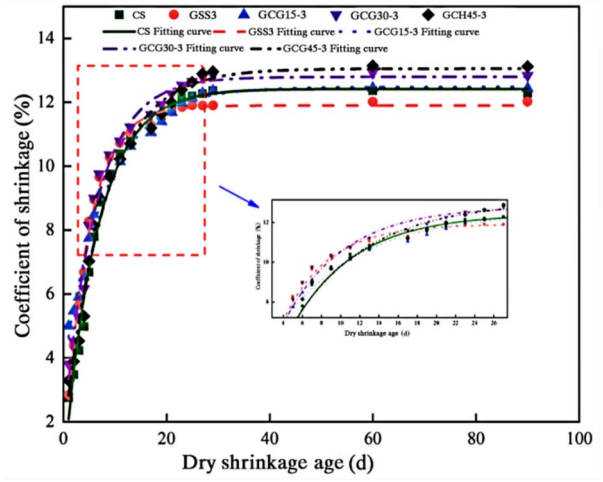

Fig. 24. The curve of dry shrinkage coefficient of different substitution amount with age.

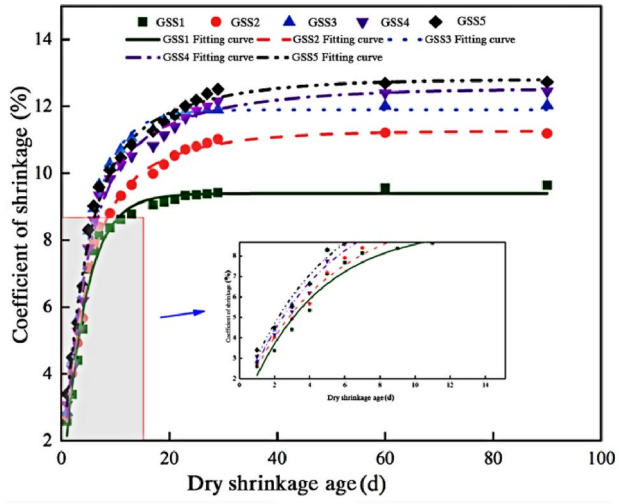

Fig. 25. Curve of drying shrinkage coefficient of different geopolymer dosage with age.

Peer group	Fitting equation	R^2
CS	$y = 177.76\left(1 - e^{\left(\frac{-x}{9.14}\right)}\right) - 14.458$	0.9956
GSS1	$y = 18.80\left(1 - e^{\left(-\frac{x}{40.86}\right)}\right) + 94.02\left(1 - e^{\left(-\frac{x}{5.63}\right)}\right) - 12.923$	0.9943
GSS2	$y = 42.273\left(1 - e^{\left(-\frac{x}{4.05}\right)}\right) + 90.786\left(1 - e^{\left(-\frac{x}{11.93}\right)}\right) - 1\,1.309$	0.9975
GSS3	$y = 50.995\left(1 - e^{\left(-\frac{x}{14.15}\right)}\right) + 108.130\left(1 - e^{\left(-\frac{x}{5.70}\right)}\right) - 14.952$	0.9985
GSS4	$y = 81.852\left(1 - e^{\left(-\frac{x}{4.73}\right)}\right) + 106.959\left(1 - e^{\left(-\frac{x}{13.72}\right)}\right) - 16.401$	0.9972
GSS5	$y = 79.237\left(1 - e^{\left(-\frac{x}{4.12}\right)}\right) + 128.628\left(1 - e^{\left(-\frac{x}{12.80}\right)}\right) - 18.385$	0.9967
GSG15-3	$y = 159.201\left(1 - e^{\left(\frac{-x}{9.88}\right)}\right) - 2.452$	0.9977
GSG30-3	$y = 69.396\left(1 - e^{\left(-\frac{x}{11.26}\right)}\right) + 115.489\left(1 - e^{\left(-\frac{x}{15.67}\right)}\right) - 11.548$	0.9966
GSG45-3	$y = 206.751\left(1 - e^{\left(\frac{-x}{10.363}\right)}\right) - 10.472$	0.9968

Table 15. Fitting results of dry shrinkage of inorganic binder stabilized materials with different ratios.

Peer group	Fitting equation	R^2
CS	$y = 0.714\left(1 - e^{\left(-\frac{x}{15.86}\right)}\right) + 2.791\left(1 - e^{\left(-\frac{x}{2.40}\right)}\right) - 0.192$	0.9956
GSS1	$y = 1.981\left(1 - e^{\left(-\frac{x}{2.37}\right)}\right) + 0.713\left(1 - e^{\left(-\frac{x}{17.97}\right)}\right) - 0.151$	0.9983
GSS2	$y = 0.737\left(1 - e^{\left(-\frac{x}{17.22}\right)}\right) + 2.123\left(1 - e^{\left(-\frac{x}{2.43}\right)}\right) - 0.133$	0.9982
GSS3	$y = 2.342\left(1 - e^{\left(-\frac{x}{2.32}\right)}\right) + 0.849\left(1 - e^{\left(-\frac{x}{16.86}\right)}\right) - 0.182$	0.9985
GSS4	$y = 0.906\left(1 - e^{\left(-\frac{x}{16.81}\right)}\right) + 2.77\left(1 - e^{\left(-\frac{x}{2.41}\right)}\right) - 0.201$	0.9983
GSS5	$y = 2.922\left(1 - e^{\left(-\frac{x}{2.42}\right)}\right) + 0.986\left(1 - e^{\left(-\frac{x}{16.39}\right)}\right) - 0.183$	0.9985
GSG15-3	$y = 0.843\left(1 - e^{\left(-\frac{x}{17.10}\right)}\right) + 2.510\left(1 - e^{\left(-\frac{x}{2.47}\right)}\right) - 0.145$	0.9985
GSG30-3	$y = 2.582\left(1 - e^{\left(-\frac{x}{2.45}\right)}\right) + 0.937\left(1 - e^{\left(-\frac{x}{17.88}\right)}\right) - 0.139$	0.9984
GSG45-3	$y = 3.091\left(1 - e^{\left(-\frac{x}{2.39}\right)}\right) + 0.877\left(1 - e^{\left(-\frac{x}{17.77}\right)}\right) - 0.213$	0.9982

Table 16. Fitting results of water loss rate of inorganic binder stabilized materials with different ratios.

be seen that the optimal water content of the GSS3 group is 4.0% less than 4.4% of the CS group. In the process of early strength formation, the water required for the reaction of the cementitious material is mainly provided by the water inside the mixture, so the water loss rate of the GSS is lower than that of the cement stabilized crushed stone. The evaporation of water will cause the water loss of the gel, and the colloidal particles that lose the water film will be subjected to molecular attraction, resulting in volume shrinkage. The increase of water loss rate leads to the increase of dry shrinkage coefficient of inorganic binder stabilized materials.

Peer group	Fitting equation	R^2
CS	$y = 46.192\left(1 - e^{\left(-\frac{x}{7.43}\right)}\right) - 5.368$	0.9883
GSS1	$y = 5.303\left(1 - e^{\left(-\frac{x}{58.38}\right)}\right) + 25.211\left(1 - e^{\left(-\frac{x}{4.59}\right)}\right) - 4.812$	0.9827
GSS2	$y = 11.552\left(1 - e^{\left(-\frac{x}{18.42}\right)}\right) + 23.565\left(1 - e^{\left(-\frac{x}{4.62}\right)}\right) - 4.476$	0.9910
GSS3	$y = 36.059\left(1 - e^{\left(-\frac{x}{5.04}\right)}\right) + 6.570\left(1 - e^{\left(-\frac{x}{30.89}\right)}\right) - 6.022$	0.9914
GSS4	$y = 15.844\left(1 - e^{\left(-\frac{x}{20.92}\right)}\right) + 34.372\left(1 - e^{\left(-\frac{x}{4.59}\right)}\right) - 6.686$	0.9881
GSS5	$y = 36.609\left(1 - e^{\left(-\frac{x}{4.40}\right)}\right) + 18.271\left(1 - e^{\left(-\frac{x}{19.05}\right)}\right) - 4.582$	0.9885
GSG15-3	$y = 22.614\left(1 - e^{\left(-\frac{x}{4.64}\right)}\right) + 20.422\left(1 - e^{\left(-\frac{x}{14.16}\right)}\right) - 3.033$	0.9924
GSG30-3	$y = 14.012\left(1 - e^{\left(-\frac{x}{18.84}\right)}\right) + 35.316\left(1 - e^{\left(-\frac{x}{5.26}\right)}\right) - 5.648$	0.9871
GSG45-3	$y = 31.016\left(1 - e^{\left(-\frac{x}{5.39}\right)}\right) + 24.111\left(1 - e^{\left(-\frac{x}{15.089}\right)}\right) - 5.756$	0.9976

Table 17. Fitting results of drying shrinkage strain of inorganic binder stabilized materials with different ratios.

Peer group	Fitting equation	R^2
CS	$y = -12.035\left(1 - e^{\left(\frac{x}{6.55}\right)}\right)$+12.419	0.9870
GSS1	$y = 9.226\left(1 - e^{\left(-\frac{x}{4.14}\right)}\right) + 0.170$	0.9756
GSS2	$y = 7.491\left(1 - e^{\left(-\frac{x}{4.08}\right)}\right) + 3.051\left(1 - e^{\left(-\frac{x}{13.89}\right)}\right) + 0.715$	0.9917
GSS3	$y = 11.415\left(1 - e^{\left(-\frac{x}{4.673}\right)}\right) + 0.485$	0.9948
GSS4	$y = 2.913\left(1 - e^{\left(-\frac{x}{18.49}\right)}\right) + 8.926\left(1 - e^{\left(-\frac{x}{4.23}\right)}\right) + 0.686$	0.9884
GSS5	$y = 8.528\left(1 - e^{\left(-\frac{x}{4.00}\right)}\right) + 3.321\left(1 - e^{\left(-\frac{x}{15.81}\right)}\right) + 0.952$	0.9883
GSG15-3	$y = -8.842\left(1 - e^{\left(-\frac{x}{8.27}\right)}\right) + 12.485$	0.9901
GSG30-3	$y = -11.093\left(1 - e^{\left(-\frac{x}{6.31}\right)}\right) + 12.796$	0.9838
GSG45-3	$y = -11.603\left(1 - e^{\left(-\frac{x}{7.88}\right)}\right) + 13.052$	0.9854

Table 18. Fitting results of dry shrinkage coefficient of inorganic binder stabilized materials with different proportions.

Different coal gangue substitution amount

Figures 18, 20, 22 and 24 also reflect the variation of dry shrinkage, water loss rate, dry shrinkage strain and dry shrinkage coefficient of geopolymer stabilized coal gangue with different coal gangue substitution rates with the increase of age, all of which show an upward trend, and increase rapidly in the early stage and tend to be gentle after 28 days. Comprehensive analysis shows that with the increase of coal gangue substitution rate, the dry shrinkage, water loss rate, dry shrinkage strain and dry shrinkage coefficient of geopolymer stabilized coal gangue increase. The dry shrinkage of geopolymer stabilized coal gangue with substitution rate of 15%, 30% and 45% increases by 10.3%, 20.0% and 35.8% respectively compared with that of 0%. The water loss rate increased by 6.9%, 12.6% and 24.9% respectively. The dry shrinkage strain increased by 10.3%, 20.1% and 35.8%, respectively. The dry shrinkage coefficient increased by 3.4%, 6.7% and 9.1%, respectively. This is because the coal gangue itself is porous and has a high water absorption rate, resulting in a higher optimum water content of the geopolymer-stabilized coal gangue material. Correspondingly, in the strength formation stage, the water loss rate will also increase. Secondly, the surface of the coal gangue may dissolve in the alkaline environment. The participation of silicon and aluminum elements in the polymerization reaction will also absorb part of the water, resulting in a larger interaction between the particles inside the specimen, showing a greater shrinkage stress. In addition, the anti-deformation ability of coal gangue is worse than that of natural gravel, so the drying shrinkage coefficient increases with the increase of coal gangue substitution rate.

Different amount of geopolymer

It can be seen from Figs. 19, 21, 23 and 25 that the dry shrinkage, water loss rate, dry shrinkage strain and dry shrinkage coefficient of GSS increase with the increase of geopolymer content, and the early growth rate is faster. This is because with the increase of the amount of geopolymer, the water required for the polymerization reaction is more and more, resulting in the increase of the water loss rate of the geopolymer stabilized macadam material. Secondly, the increase of the amount of geopolymer will make the polymerization reaction more intense, the spacing between the powder particles in the mixture becomes smaller, and the interaction force between the particles is enhanced, so that the shrinkage stress in the specimen increases, and the dry shrinkage is increasing. The fitting equation shown in Table 15 can effectively characterize the relationship between age and dry shrinkage. In addition, it can be seen from the compaction test results that with the increase of geopolymer content, the optimum water content of GSS increases continuously. Because most of the water required for early water evaporation and geopolymerization reaction comes from free water in the mixture, the water loss rate increases. Table 16 is the fitting curve equation of water loss rate of geopolymer stabilized coal gangue with different mix ratios, and R^2 is greater than 0.99. The relationship between water loss rate and dry shrinkage age can be well characterized by fitting equation and fitting curve.According to the drying shrinkage mechanism, the higher the water loss rate, the higher the internal humidity of the specimen at the end of the month, the loss of water will cause the formation of water–air meniscus in the capillary, resulting in hydrostatic tensile stress, resulting in volume shrinkage. The macroscopic performance is that the greater the water loss rate, the drying shrinkage is about obvious, so the geopolymer stabilized coal gangue material will increase with the increase of the amount of geopolymer, and the drying shrinkage coefficient will continue to increase. Further analysis of Fig. 25 shows that when the amount of geopolymer is from 5 to 7%, the 90 d drying shrinkage coefficient is not much different. This is because when the amount of geopolymer is large, the geopolymer stabilized macadam has a strong polymerization reaction in the early stage, and the later strength is basically stable. The influence of the external environment on it will also become smaller.

The freeze-drying shrinkage test of slag-based geopolymer stabilized coal gangue materials with different amounts of rubber powder was carried out. The dry shrinkage and water loss rate of different drying ages were recorded according to the specifications. The test results and Figs. 26 and 27, the fitting curve equation is shown

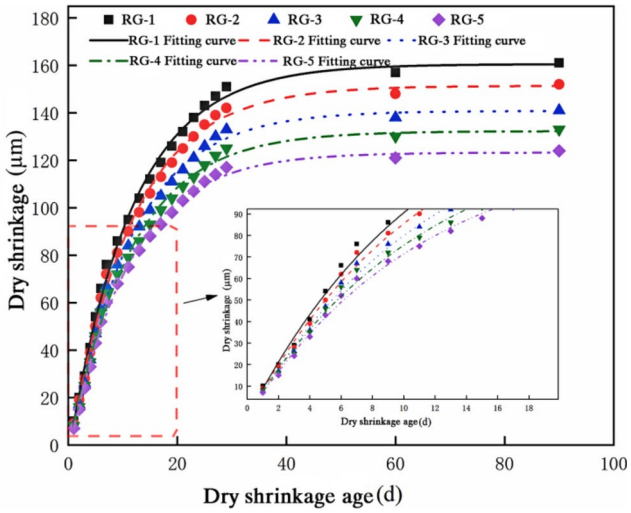

Fig. 26. Dry shrinkage of geopolymer stabilized coal gangue material mixed with rubber powder.

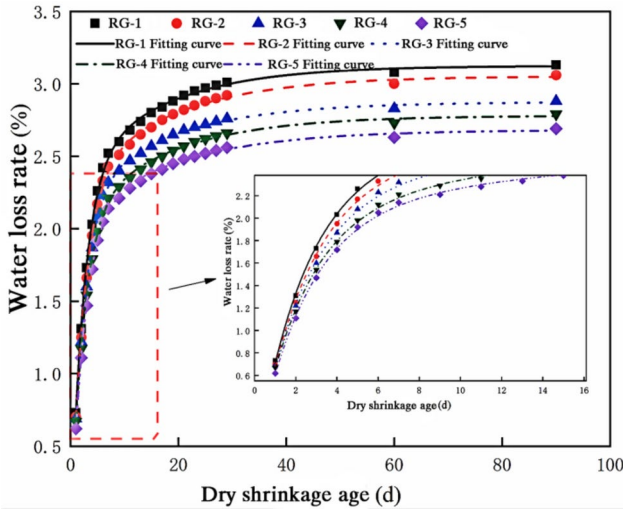

Fig. 27. Water loss rate of geopolymer stabilized coal gangue material mixed with rubber powder.

Peer group	Fitting equation	R^2
RG-1	$y=-165.358\left(1-e^{\left(-\frac{x}{11.62}\right)}\right)+160.512$	0.9962
RG-2	$y=-156.180\left(1-e^{\left(-\frac{x}{11.57}\right)}\right)+151.382$	0.9968
RG-3	$y=-145.916\left(1-e^{\left(-\frac{x}{11.43}\right)}\right)+140.805$	0.9975
RG-4	$y=-135.880\left(1-e^{\left(-\frac{x}{11.46}\right)}\right)+132.262$	0.9955
RG-5	$y=-127.571\left(1-e^{\left(-\frac{x}{11.10}\right)}\right)+123.251$	0.9965

Table 19. Dry shrinkage fitting equation.

Peer group	Fitting equation	R^2
RG-1	$y=-2.197e^{-\frac{x}{2.45}}-0.652e^{-\frac{x}{18.41}}+2.682$	0.9989
RG-2	$y=-2.185e^{-\frac{x}{2.35}}-0.736e^{-\frac{x}{16.94}}+2.781$	0.9988
RG-3	$y=-2.355e^{-\frac{x}{2.44}}-0.674e^{-\frac{x}{17.391}}+2.874$	0.9988
RG-4	$y=-2.469e^{-\frac{x}{2.41}}-0.783e^{-\frac{x}{17.38}}+3.052$	0.9984
RG-5	$y=-2.555e^{-\frac{x}{2.37}}-0.781e^{-\frac{x}{16.04}}+3.123$	0.9981

Table 20. Fitting equation of water loss rate.

in Tables 19 and 20. The results of shrinkage strain and shrinkage coefficient obtained by calculation are shown in Figs. 28 and 29, and the fitting curve equation is shown in Tables 21 and 22.

It can be seen from Figs. 26 and 27 that the dry shrinkage and water loss rate of geopolymer stabilized coal gangue materials with rubber powder increase with the increase of dry shrinkage age, but the growth rate shows different changing rules. The fitting equations in Tables 19 and 20 can well reflect the relationship between dry shrinkage, water loss rate and dry shrinkage age. Combined with the fitting equation, it can be seen that the dry shrinkage of the five groups of content reached the peak at 4–6d, and the growth rate of the water loss rate showed a downward trend, which was smaller than that of the geopolymer stabilized coal gangue material without rubber powder. In addition, with the increase of rubber powder content, the final dry shrinkage and water loss rate of geopolymer stabilized coal gangue materials continue to decrease.

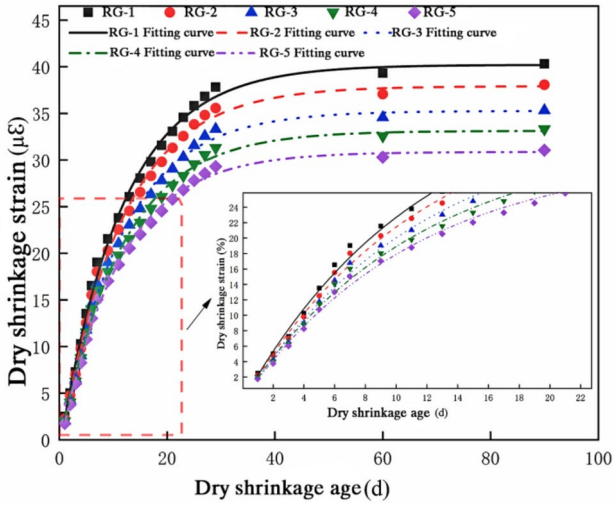

Fig. 28. Dry shrinkage strain of geopolymer stabilized coal gangue material mixed with rubber powder.

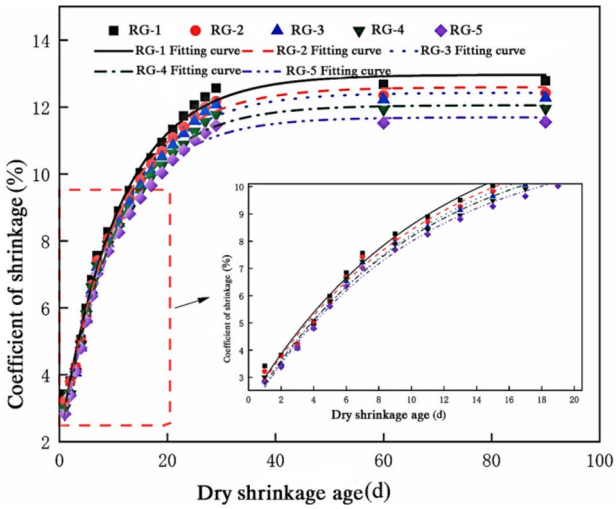

Fig. 29. Dry shrinkage coefficient of geopolymer stabilized coal gangue material mixed with rubber powder.

Peer group	Fitting equation	R^2
RG-1	$y = -41.415e^{-\frac{x}{11.62}} + 40.198$	0.9962
RG-2	$y = -39.113e^{-\frac{x}{11.56}} + 37.910$	0.9961
RG-3	$y = -36.543e^{-\frac{x}{11.43}} + 35.263$	0.9968
RG-4	$y = -34.030e^{-\frac{x}{11.46}} + 33.124$	0.9966
RG-5	$y = -31.949e^{-\frac{x}{11.09}} + 30.864$	0.9968

Table 21. Dry shrinkage strain fitting equation.

Through the analysis of Table 20 and Figs. 28 and 29, it can be seen that the dry shrinkage strain and dry shrinkage coefficient of the geopolymer stabilized coal gangue material with rubber powder increase with the increase of dry shrinkage age, which is similar to the GSG30-3 group without rubber powder. In the first 20 days, the growth rate increased rapidly, the growth rate slowed down from 20 to 28 days, and the growth rate tended to be stable after 28 days. The fitting equations shown in Tables 21 and 22 can accurately express the relationship between dry shrinkage strain and dry shrinkage coefficient and dry shrinkage age. In addition, it can be seen that the total dry shrinkage strain and dry shrinkage coefficient of RG-1, RG-2, RG-3, RG-4 and RG-5 decrease with the increase of rubber powder content, and the larger the content, the greater the decrease. The total dry

Peer group	Fitting equation	R^2
RG-1	$y = -10.942e^{-\frac{x}{10.91}} + 12.962$	0.9937
RG-2	$y = -10.634e^{-\frac{x}{10.72}} + 12.593$	0.9951
RG-3	$y = -10.734e^{-\frac{x}{10.63}} + 12.428$	0.9953
RG-4	$y = -10.239e^{-\frac{x}{10.34}} + 12.053$	0.9941
RG-5	$y = -9.996e^{-\frac{x}{10.07}} + 11.692$	0.9958

Table 22. Dry shrinkage coefficient fitting equation.

shrinkage strains were 40.32 με, 38.07 με, 35.31 με, 33.31 με and 31.05 με, respectively, which were 7.5%, 12.6%, 19.0%, 23.5% and 28.87% lower than those in the GSG30-3 group. The dry shrinkage coefficients were 12.78%, 12.42%, 12.27%, 11.95% and 11.55%, respectively, which were 0.46%, 3.27%, 4.44%, 6.93% and 10.05% lower than those in the GSG30-3 group. The reason may be that the incorporation of rubber powder reduces the water content of the geopolymer stabilized coal gangue specimen, so that the water loss rate of the mixture with rubber powder is less than that of the mixture without rubber powder. On the other hand, as an elastic material, rubber powder can absorb and disperse the shrinkage stress generated by the geopolymer stabilized coal gangue material during the drying process, and reduce the capillary tension, adsorbed water and intermolecular force caused by water evaporation to a certain extent, thereby reducing the drying shrinkage. The dry shrinkage coefficient of the specimen mixed with rubber powder increases slowly with the age, which is beneficial to delay the cracking of the base layer. As the volume of rubber becomes larger, the improvement effect on the dry shrinkage characteristics is more obvious.

Micro performance analysis

Figure 30 is the micro-morphology of 7 d cement mortar samples with different magnifications after mechanical test.

The surface of cement particles at 7 d age may be covered with some initially formed hydration products, such as hydrated calcium silicate (C–S–H) gel. These hydration products show a relatively small morphology and have not yet formed a complete internal structure. It can be seen from Fig. 30a and b that the surface of the cement mortar sample is relatively flat under the magnification of 500 times and 1000 times, and there is no obvious grain and gully feeling, indicating that the compound formed in the early stage of the reaction of the cementitious material forms the early strength. It can be seen from Fig. 30c and d that the morphological characteristics of hydration products can be seen more clearly due to the increase of multiples. Due to the large gap between the solid phases in the cement paste at the initial stage of hydration, the hydrate is less, the growth space is large, and it is easy to identify. Fibrous and grid hydrated calcium silicate hydrate (C–S–H gel) and flake Ca $(OH)_2$ grow well and have a complete shape. In addition, there is a large amount of acicular ettringite formation.

Figure 31 shows the micro-morphology of geopolymer mortar samples after mechanical tests at 7 d ages with different magnifications.

The main hydration products in the geopolymer system include hydrated calcium aluminosilicate (C–A–S–H) and hydrated sodium aluminosilicate (N–A–S–H) gels. Unlike traditional cement-based composites, strength development does not depend on the formation of hydrated calcium silicate (C–S–H), but on the quality and quantity of C–A–S–H/N–A–S–H gels[37,38]. It can be seen from Fig. 31a that the morphology of the slag-based geopolymer has a lamellar structure similar to that of the slag powder particles, with a dense microstructure and a complete structure, which means that the cementitious material fully reacts to form a dense C–A–S–H structure. It can be seen from Fig. 31b that the fly ash particles in the two states, the unreacted fly ash particles are fuzzy spherical particles, and the partially reacted fly ash is similar to a ring, and the unreacted slag powder particles are irregular blocks with layered silicate accumulation, which gradually disappear during the hydration process. The reaction of fly ash particles is carried out from the surface to the inside and is surrounded by hydration products. Fly ash particles have smooth shells and porous interiors. Subsequently, the fly ash particles are filled with hydrated products or replaced by hydrated products. This is because the calcium content of slag powder is higher than that of fly ash, and the early strength is formed quickly. The dissolution of silicon and aluminum in fly ash is very slow, and it can be clearly seen from Fig. 31c and d. When calcium ions are dissolved from the raw material slag powder, they preferentially combine with the Si ions in the solution and precipitate as hydrated calcium silicate, which may be rich in alkali. Because of its low solubility, the precipitation of C–S–H is better than that of Ca $(OH)_2$.

Figures 32 and 33 are the EDS spectra of cement mortar and geopolymer, respectively. In order to verify the composition of spherical, flake and flocculent structures, the surface distribution of geopolymer materials was tested. The test results are shown in Fig. 34.

By analyzing Figs. 32 and 33, it can be seen that the main elements contained in cement are O (50.7%), C (16.7%), A1 (2.8%), Si (11.2%), Ca (14.6%), etc., and the main elements contained in geopolymer are Fe (0.11%), C (37.1%), A1 (0.44%), Si (0.87%), Ca (61.43%), etc.

Combined with the surface distribution results of Fig. 34, it can be seen that the two cementitious materials are mainly O, Al, Si, Mg, Ca, K and Fe. The uniformity of the distribution of geopolymer materials has a great influence on the formation of strength. Therefore, in order to investigate the distribution of each element in the

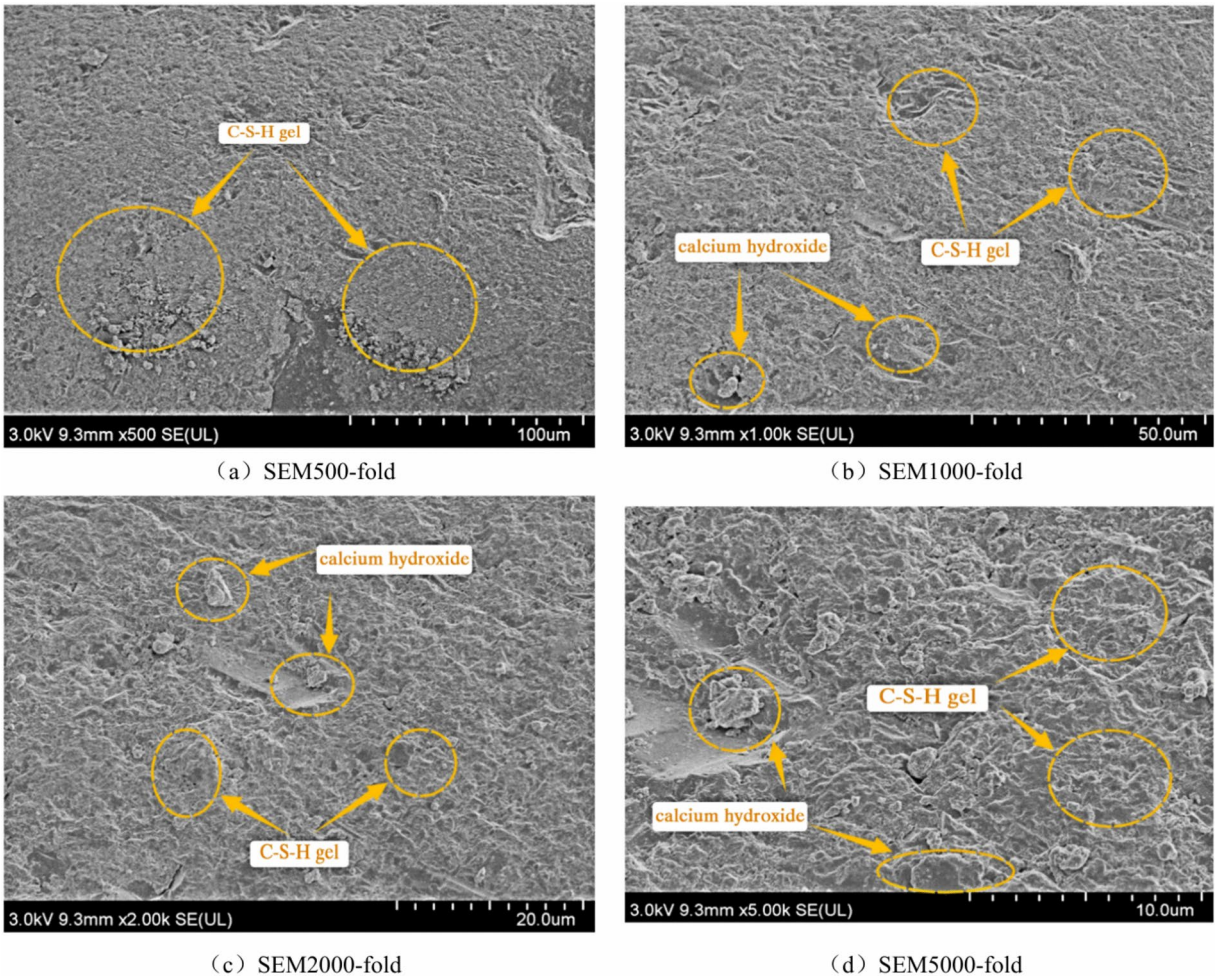

Fig. 30. Microscopic morphology of cement mortar samples at 7 d age.

cementitious material powder, the surface of the cementitious material powder is magnified to 1000 times. It can be seen from the surface distribution of Ca, C, Al, Si and Fe five elements. The distribution of each element component of the geopolymer cementitious material is relatively uniform, and no component segregation occurs. This further indicates that the geopolymer material has good dispersibility after the polymerization reaction and can fully cement with the aggregate, indicating that C–A–S–H and N–A–S–H are the main components of the geopolymer gel.

Figure 35 is the scanning electron microscope micro-morphology of the geopolymer-stabilized coal gangue of the RG-4 group with rubber powder, and Fig. 36 is a simplified schematic diagram of rubber powder in the geopolymer-stabilized coal gangue material.

It can be seen from Fig. 35 that the rubber powder is wrapped by C–S–H and C–A–S–H gels, and the rubber powder is filled in pores and cracks, indicating that the interface between the rubber powder and the geopolymer reaction product is good, and the thickness of the interface transition zone is small.

Analysis of Fig. 36, combined with Fig. 35, it can be seen that when subjected to external forces, the particles will overcome the frictional resistance, move and fill each other to form a new arrangement. In this process, the particles will deform, the voids will decrease, and the density will increase. When the external force increases, the energy of particle movement and filling will also increase, making the material more dense. This densification process helps to resist shrinkage deformation. At the same time, rubber powder has excellent tensile and deformation ability. When the shrinkage deformation of geopolymer stabilized coal gangue occurs during the formation of strength, the rubber powder can use its elastic properties to absorb part of the shrinkage stress, thereby reducing the shrinkage deformation of geopolymer stabilized coal gangue.

Conclusion

(1) With the same amount of cementitious materials, the compressive strength, indirect tensile strength and compressive resilient modulus of geopolymer stabilized macadam are slightly higher than those of cement stabilized macadam. Because the three-dimensional network structure of geopolymer can effectively resist water erosion and geopolymer has the characteristics of early strength, it can effectively reduce the damage

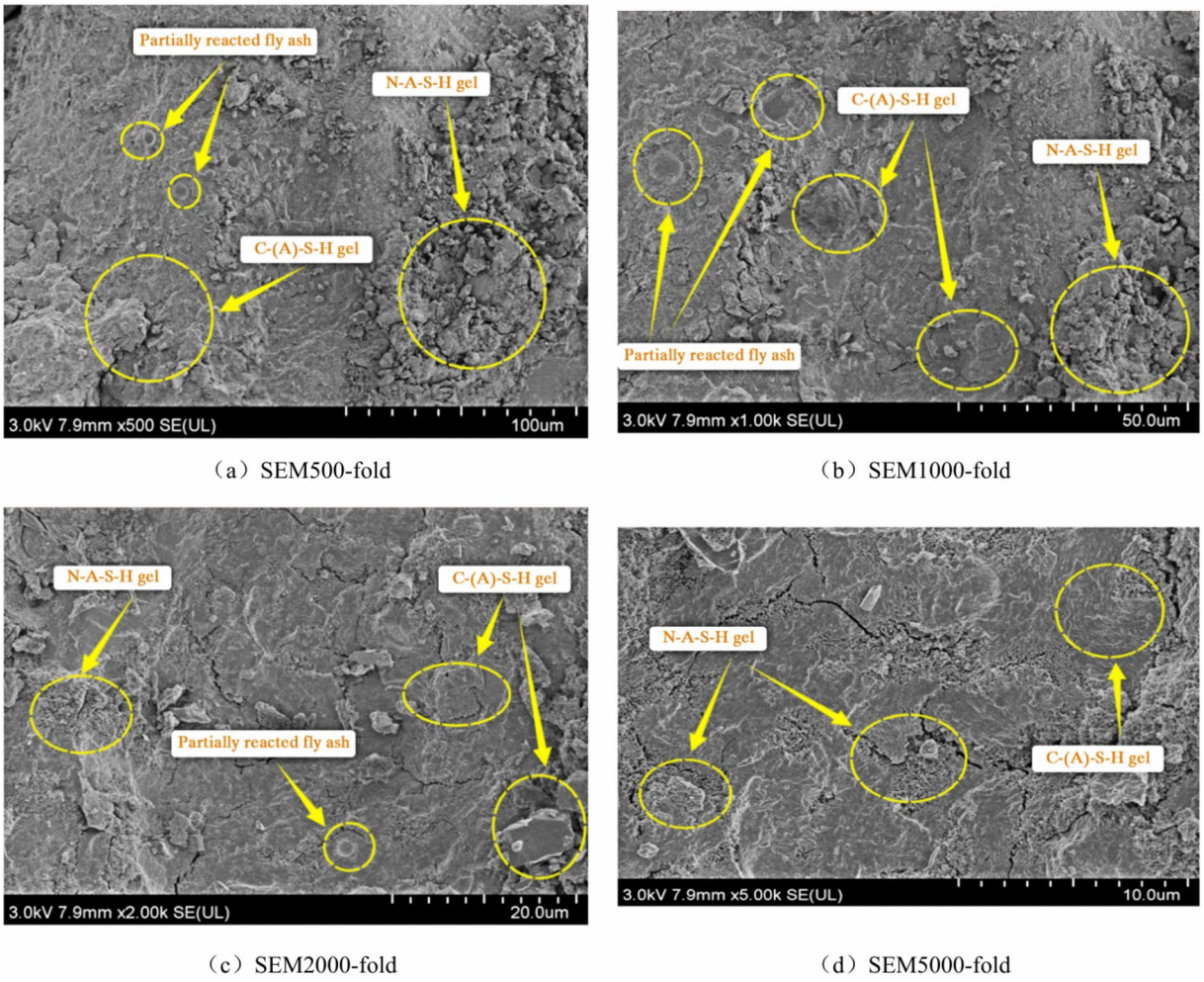

Fig. 31. Microscopic morphology of geopolymer mortar samples at 7 d age.

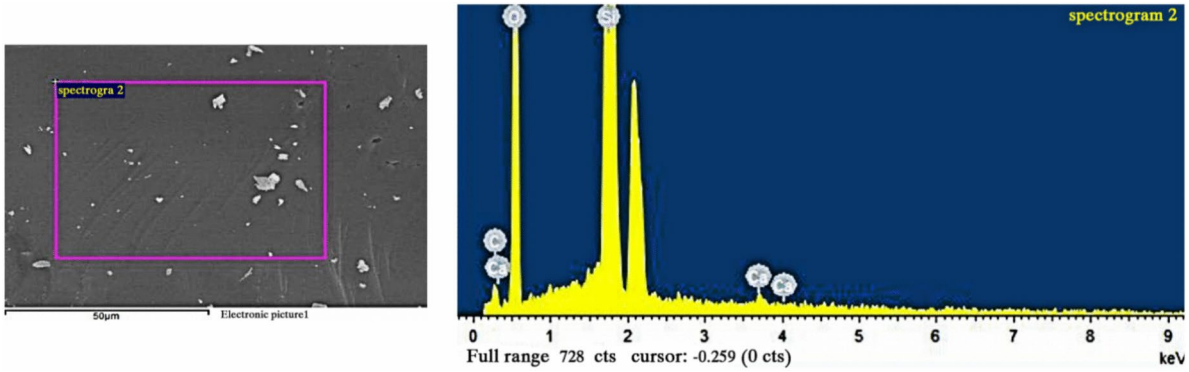

Fig. 32. EDS spectra of cement mortar.

of freeze–thaw cycle to the material structure and can just resist the internal stress of the specimen due to water loss. The frost resistance and dry shrinkage performance are also better than those of cement stabilized macadam.

(2) With the increase of the amount of geopolymer, the strength of GSS is also increasing, and the strength growth rate is faster when the amount of geopolymer is 3–5%, and the strength change rate of 6–7% is lower. The compressive resilient modulus of slag-based geopolymer stabilized materials increases linearly with the increase of geopolymer content. Although its frost resistance is also getting better, the rate of increase is

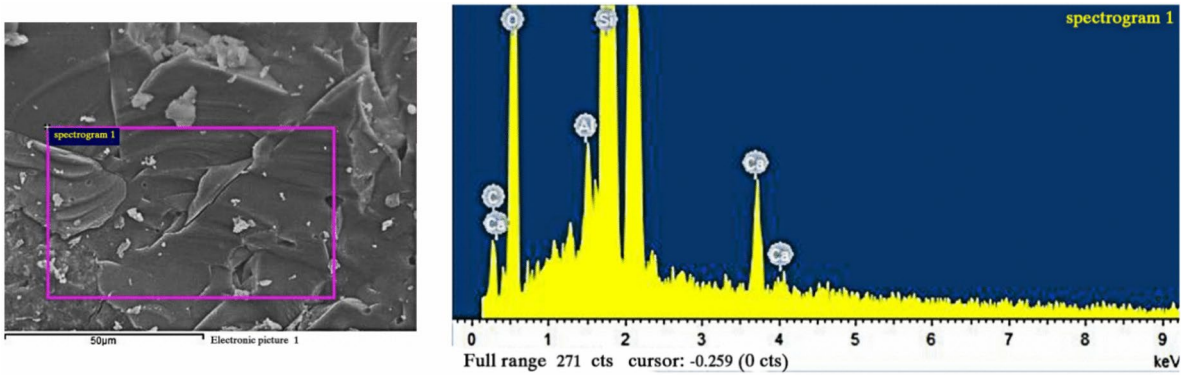

Fig. 33. EDS spectra of geopolymer mortar.

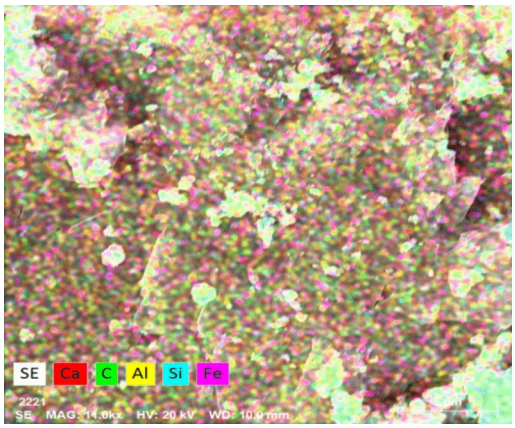

Fig. 34. The schematic diagram of the elements contained in geopolymer cementitious materials.

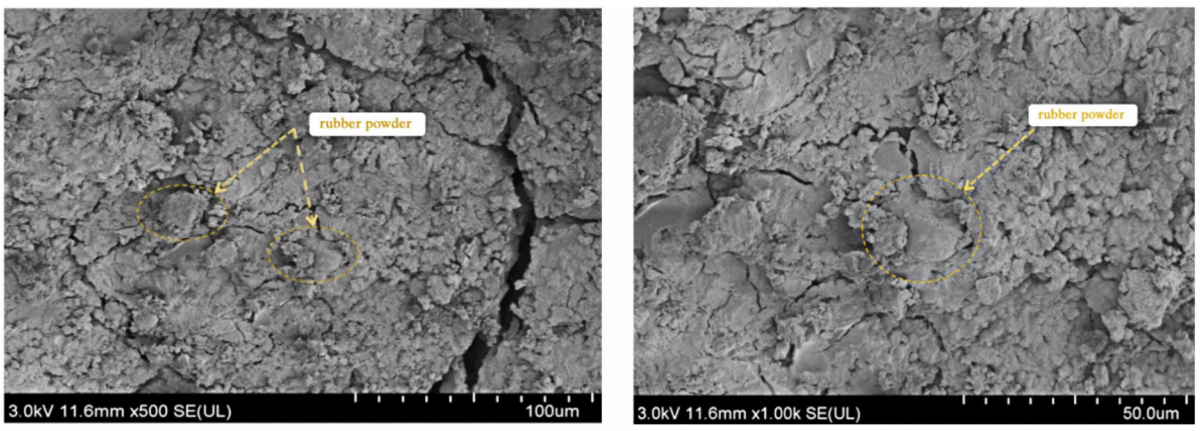

（a）SEM500-fold　　（a）SEM1000-fold

Fig. 35. RG-4 groups of geopolymer stabilized coal gangue material microscopic morphology.

gradually decreasing. In addition, the drying shrinkage coefficient is increasing, and the anti-drying shrinkage performance of the specimen is reduced.

(3) The addition of coal gangue is unfavorable to the compressive strength and indirect tensile strength of the material, and the greater the content, the more the mechanical properties of the specimen decrease, and the compressive resilient modulus of the slag-based polymer stabilized coal gangue mixture also shows a

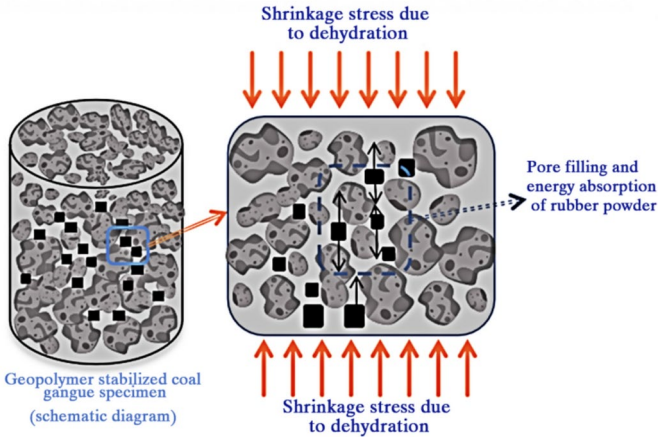

Fig. 36. Simplified schematic diagram of rubber powder in geopolymer stabilized coal gangue specimen.

downward trend. Because the coal gangue itself contains more voids, the geopolymer stabilized coal gangue material may form weak points or voids inside, thereby increasing its permeability and water absorption capacity. Therefore, with the increase of coal gangue content, its frost resistance and dry shrinkage performance are worse than the benchmark group.

(4) The incorporation of rubber powder will have a negative impact on the mechanical properties of slag-based geopolymer-stabilized coal gangue materials. With the increase of rubber powder content, the mass loss rate of slag-based geopolymer-stabilized coal gangue materials after freeze–thaw cycles continues to increase, and the greater the amount of rubber powder, the more obvious the BDR of the mixture decreases. However, as an elastic material, rubber powder can absorb and disperse stress and reduce the shrinkage stress generated by geopolymer-stabilized coal gangue materials during drying. Therefore, the addition of rubber powder can significantly improve the dry shrinkage performance of geopolymer stabilized coal gangue materials. The optimum dosage is 1.2%, and the dry shrinkage coefficient is reduced by 12.1%.

(5) Calcium silicate hydrate gel (C–S–H) and calcium aluminosilicate hydrate gel (C–A–S–H) were formed by polycondensation of slag powder and silica contained in water glass solution. The bonding effect of C–S–H generated by slag can be used as a condensation nucleus to promote the formation of N–A–S–H gel from fly ash. The rubber powder not only has a filling effect on the voids in the geopolymer stabilized coal gangue material, but also the movement and filling energy of the rubber powder particles will increase, thereby improving the compressive resilience modulus of the geopolymer stabilized coal gangue material and reducing the shrinkage deformation of the geopolymer stabilized coal gangue.

(6) In this paper, slag and fly ash are used as precursors to prepare geopolymers by alkali activation. Due to the diversity of raw materials and preparation methods of geopolymers, there are also differences between alkali activation and acid activation. Therefore, it is necessary to prepare geopolymers with different raw materials to obtain better cementitious materials.

Data availability

Some or all data, models, or code that support the findings of thisstudy are available from the corresponding author upon reasonable request.

Received: 25 September 2024; Accepted: 23 January 2025
Published online: 10 February 2025

References

1. Ni, C., Wang, E. & Zhou, J. Geopolymer green cementitious materials in the 21st century. *Adv. Mater. Ind.* **6**, 24–28 (2003).
2. Meyer, C. The greening of the concrete industry. *Cem. Concr. Compos.* **31**(8), 601 (2009).
3. Habert, G., Lacaillerie, J. B. D. E. & Roussel, N. An environmental evaluation of geopolymer based concrete production: Reviewing current research trends. *J. Clean. Prod.* **19**(11), 1229–1238 (2011).
4. Mclellan, B. C. et al. Costs and carbon emissions for geopolymer pastes in comparison to ordinary portland cement. *J. Clean. Prod.* **19**(9–10), 1080 (2011).
5. Mishra, J., Das, S., Krishna, R. S. & Bharadwaj, N. Utilization of ferrochrome ash as a source material for production of geopolymer concrete for a cleaner sustainable environment. *Indian Concr. J.* **94**(7), 40–49 (2020).
6. van Deventer, K. J. S. J., Provis, J. L. & Duxson, P. Technical and commercial progress in the adoption of geopolymer cement. *Miner. Eng.* **29**, 89–104 (2012).
7. Li, J. et al. Current situation analysis and proposed countermeasures of coal resource development and management. *China Coal* **49**(9), 1–6 (2023).
8. Wang, L. et al. Research on multi-energy complementary energy supply in coal mines in western China under the goals of carbon peak and carbon neutrality. *China Coal* **49**(10), 36–42 (2023).
9. Cheng, K. et al. Research on application of the standards of "three rates" for rational development and utilization of coal resources. *China Coal* **50**(01), 15–20 (2024).
10. *BP Statistical Review of World Energy 2023* (2018).

11. Jabłońska, B. et al. The structural and surface properties of natural and modified coal gangue. *J. Environ. Manag.* **190**, 80–90 (2017).
12. Liu, X. Promote the reclamation of coal gangue ground backfill land. China Mining News 2024-03-12(003).
13. Škvára, F. et al. Microstructure of geopolymer materials based on fly ash. *Ceram Silikaty* **50**, 208–215 (2006).
14. Komnitsas, K. & Zaharaki, D. Geopolymerisation: a review and prospect for the minerals industry. *Miner. Eng.* **20**, 1261–1277 (2007).
15. Ismail, I. et al. Modification of phase evolution in alkali-activated blast furnace slag by the incorporation of fly ash. *Cem. Concr. Compos.* **45**, 125–135 (2014).
16. Jena, S. & Panigrahi, R. Performance assessment of geopolymer concrete with partial replacement of ferrochrome slag as coarse aggregate. *Constr. Build. Mater.* **220**, 525–537 (2019).
17. Yi, F. et al. Mechanical properties and mechanism analyses of rice husk ash geopolymer solidified soil. *Hydrogeol. Eng. Geol.* **49**(02), 94–101 (2022).
18. Liu, Z. et al. Preparation of Rice Husk Ash and lts Effect on Mechanical Properties of Geopolymer. *Bull. Chin. Ceram. Soc.* **39**(12), 3881–3888 (2020).
19. Ding, Z. et al. Study on properties of slag and fly ash based geopolymer. *Concrete* **7**, 125–129 (2022).
20. Liu, G. et al. Hydration behavior and mechanical properties of alkaline excited slag-fly ash-metakaolin geopolymer. *Bull. Chin. Ceram. Soc.* **42**(06), 2106–2114 (2023).
21. Zhang, T. Road performance analysis of cement stabilized coal gangue mixture. *West. China Commun. Sci. Technol.* **11**, 27–29 (2023).
22. Liu, Y. *Mix Design and Mechanics of Cement Stabilized Coal Gangue Brick Mixture* (North University of China, Taiyuan, 2024).
23. Tong, Y. et al. Frost resistance test of slag coal gangue mixture stabilized by cement and fly ash. *China Sciencepaper* **17**(10), 1078–1083 (2022).
24. Di, G. et al. Experimental study on mechanical properties of road coal gangue. *Railw. Eng.* **8**, 127–129 (2011).
25. Wang, J. et al. Effect of excitation stirring on compressive strength of cement stabilized crushed stone and coal gangue. *Bull. Chin. Ceram. Soc.* **43**(02), 757–765 (2024).
26. Li, Z. et al. Road performance analysis of cement stabilized coal gangue mixture. *Mater. Res. Express* **8**(12), 125502 (2021).
27. Guan, J. et al. An experimental study of the road performance of cement stabilized coal gangue. *Crystals* **11**, 993 (2021).
28. Zhu, Z. H. & Fang, Y. An experimental study on flexural-tensile property of cement stabilized coal gangue roadbase materials. *Appl. Mech. Mater.* **638–640**, 1536–1540 (2014).
29. Zhang, H. et al. Test research on temperature shrinkage performance of cement and cinder stabilized coal gangue base course materials. *J. Highw. Transp. Res. Dev.* **11**, 29–32 (2007).
30. Cheng, P. et al. Test on temperature shrinkage performance of lime and fly-ash stabilized coal gangue base course materials. *J. Shenyang Jianzhu Univ. Nat. Sci.* **01**, 44–48 (2008).
31. Wang, C. et al. Evaluation of skid resistance of pavement maintenance energy-absorbing seal based on surface texture characteristics. *Measurement*. **245**, 116588 (2025).
32. Fan, Z. et al. Fog seal with polymer composite modified emulsified asphalt: Road performance and environmental adaptability. *Wear*. **562**, 205672 (2025).
33. JTG 3420-2020, *Highway Engineering Cement and Cement Concrete Test Procedures* (China Communication Press, 2020).
34. JTG/T F20-2015, *Highway Pavement Base Construction Technical Rules* (China Communication Press, 2015).
35. JTG E42-2005, *Highway Engineering Aggregate Test Procedures* (China Communication Press, 2005).
36. JTG E51-2009, Test Procedure for Inorganic Binder Stabilized Materials of Highway Engineering (China Communication Press, 2009).
37. Al-Kutti, W. et al. An overview and experimental study on hybrid binders containing date palm ash, fly ash, OPC and activator composites. *Constr. Build. Mater* **159**, 567–577 (2018).
38. Ye, H. & Radlińska, A. Fly ash-slag interaction during alkaline activation: Influence of activators on phase assemblage and microstructure formation. *Constr. Build. Mater.* **122**, 594–606 (2016).

Author contributions

Writing—original draft preparation, Li, Z. X.; writing—review and editing, Guo, T. T., Y. Z. Chen.; investigation, C. Z. Fang and Nie, J. X.; discussion, Guo, T. T., Y. Z. Chen. All authors have read and agreed to the published version of the manuscript.

Funding

This work was supported by Planned project supported by science and technology innovation team of universities and colleges in Henan province: (Grant No. 24IRTSTHN011); the Central Plains Science and Technology Innovation Leader Project (Grant No. 244200510031); Henan Province's planned science and technology projects for 2025: Research on Key Technologies of Graphene Oxide/Polyurethane Synergistically Modified Asphalt.

Declarations

Competing interests

The authors declare no competing interests.

Additional information

Correspondence and requests for materials should be addressed to Y.C.

Reprints and permissions information is available at www.nature.com/reprints.

Publisher's note Springer Nature remains neutral with regard to jurisdictional claims in published maps and institutional affiliations.